Aalto University School of Engineering
Technical University of Denmark
Nordic Master in Maritime Engineering

Pablo Esquivel de Pablo

Analysis of the Shear Stress Distributions on two Ship Hull Forms

Master's Thesis
Esbo, November 16, 2013

Supervisors: Professor Jerzy Matusiak, Aalto University
Professor Poul Andersen, Technical University of Denmark
Instructor: Tommi Mikkola D.Sc., Aalto University

Aalto University School of Engineering
Technical University of Denmark
Nordic Master in Maritime Engineering

ABSTRACT OF
MASTER'S THESIS

Author: Pablo Esquivel de Pablo

Title: Analysis of the Shear Stress Distributions on two Ship Hull Forms

Date: November 16, 2013 **Pages:** vi + 74

Professorship: Naval Architecture **Code:** K211-C

Supervisors: Professor Jerzy Matusiak, Aalto University
Professor Poul Andersen, Technical University of Denmark

Instructor: Tommi Mikkola D.Sc., Aalto University

The goal of this thesis is to see the influence of the hull form on the distribution of the shear stresses. The shear stresses are computed with the CFD software OpenFOAM as solver.

Two different hulls are computed. The first hull is a modern tanker, the KVLCC2, a benchmark case well studied for the last two decades. The second hull is a cruise ferry built short time before this thesis is written. This provides two cases on the extremes of the hull shape range. The scale is also considered in the analysis of the hulls. Both hulls are computed in model and full scales.

The results are processed as coefficients, some of them widely used and some specifically developed for this thesis. The calculations required to obtain these coefficients are coded in Matlab. The validation of the results is done by comparing the tanker case with the previous work and literature. The same framework will be applied on the cruise ferry case. The shear stresses are contrasted with the expected values of a flat plate. The analysis of the distribution is divided in three steps. The first step target is to see the overall distribution on the surface. The local values are analyzed in the second step with longitudinal cuts. The third step is to see the evolution along the length of each hull.

The present work should be considered as an introduction to the analysis of the shear stresses. The approach is from the naval architecture point of view.

Keywords: cfd, shear, stresses, reynolds, ITTC, hull form factor

Language: English

Acknowledgements

The thesis was written at the Department of Applied Mechanics of Aalto University during the first semester of 2013. This thesis consummates the Nordic Master in Maritime Engineering, started in 2011 at the Technical University of Denmark.

I wish to thank my instructor D.Sc. Tommi Mikkola for giving me the opportunity and the courage to embark on this master thesis. His guidance and explanations have been decisive to complete this work.

I am grateful to my supervisors, Professor Jerzy Matusiak from Aalto and Professor Poul Andersen from DTU. To Professor Matusiak for the instructions and corrections on the thesis. To Professor Andersen for the support and guidance, during the thesis process as well as throughout my whole Master programme.

The work was supported by the Innovations and Networks programme of the Finnish Metals and Engineering Competence Cluster, FIMECC. This financial support is greatly appreciated. I would also like to thank STX Finland for providing the cruise ferry geometry and the Finnish IT Center for Science (CSC) for computing the $72.3 \cdot 10^6$ CPU seconds required in this thesis.

I want furthermore to acknowledge my colleagues Ville Viitanen and Patrik Asén for the mutual collaboration in this work and the tips and hints when the thesis got stuck.

I am also thankful to my family, friends and specially to Maria Noppenau, for their patience and for reminding me the objective of this thesis. Thanks a lot for keeping this thesis out of my head whenever I needed.

Esbo, November 16, 2013

Pablo Esquivel de Pablo

Contents

Acronyms

ATTC American Towing Tank Conference. 12

CFD Computational Fluid Dynamics. 1

DNS Direct Numerical Simulation. 1

G2000 Gothengburg 2000 Workshop on Numerical Ship Hydrodynamics [20]. 30

ITTC International Towing Tank Conference. 2, 12, 23, 50

KRISO Korean Institute of Ships and Ocean Engineering.. 19

KVLCC2 KRISO Very Large Crude Carrier. 1, 19, 22, 28

MOERI Korean Maritime and Ocean Engineering Research Institute. 1

RANS Reynolds Averaged Navier-Stokes. 1

SST Shear Stresses Transport. 13–16, 59

Glossary

AP Aft perpendicular. Located at $x = 0$. 32

C_B Block coefficient. $C_B = \frac{\nabla}{L \cdot B \cdot T}$. 19

C_F Mean skin friction coefficient. $C_F = \frac{R_F}{\frac{1}{2}\rho U_0^2 \cdot S}$. 2, 11, 46

C_{PV} Viscous pressure resistance coefficient. $C_{PV} = \frac{\int_S p \cdot \mathbf{n_x} dA}{\frac{1}{2}\rho S \cdot U_0^2}$. 8, 13

C_V Viscous resistance coefficient. $C_F = \frac{R_V}{\frac{1}{2}\rho U_0^2 \cdot S}$. 12

C_f Local skin friction coefficient. Note the case of the subindex $_f$. 9

Co Courant number. $Co = \frac{u \Delta t}{\Delta x}$. 24

Fr Froude number. $Fr = \frac{U_0}{\sqrt{g \cdot L}}$. 2

I Turbulence intensity. $I = \frac{u'}{U} = \frac{\sqrt{\frac{1}{3} u_i' \cdot u_i'}}{U}$. 15

L_F Length of the frame. $L_F = \left(\int ds \right)_{x=constant}$. 27

L_{PP} Length between perpendiculars in meters. 22, 23

L_{SS} Length of station spacing. 27

Ma Mach number. $Ma = \frac{U}{c} = \frac{U}{\sqrt{\frac{E}{\rho}}}$. 2, 4

Re Reynolds number. $Re = \frac{U_0 \cdot L}{\nu}$. 2

Re_x Reynolds number along the surface, where $x = 0$ is the leading edge. $Re = \frac{U_0 \cdot x}{\nu}$. 5

U_0 The reference velocity in $\frac{m}{s}$. 4, 9, 15

Θ Momentum thickness. $\Theta = \int_0^\infty \frac{u}{U_0} \left(1 - \frac{u}{U_0} \right) dy$. 5

$\breve{C}_f$ Averaged frame skin friction coefficient. $\breve{C}_f(x) = \frac{1}{L_F}\int C_f(x,s)\,ds$. 13, 46

$\breve{C}_{PV}$ Averaged frame viscous pressure resistance coefficient. $\breve{C}_{PV}(x) = \frac{1}{\frac{1}{2}\rho \cdot L_F \cdot U_0^2}\int p(x,s)\,n_x ds$. 13, 48

δ Boundary layer thickness. $\delta = y|_{u=0.995\cdot U_0}$. The symbol used by the ITTC is δ_{995}. 5

δ^* Displacement thickness. $\delta^* = \int_0^\infty \left(1 - \frac{u}{U_0}\right) dy$. 5

ν Kinematic viscosity of the fluid. In the case of water its value is $\nu = 1.256 \cdot 10^{-6}\frac{m^2}{s}$. 6, 9

τ_w Wall shear stress. $\tau_w = \mu\left[\frac{\partial U}{\partial y}\right]_{y=0}$. 9

k Hull form factor. 13, 46

$k-\omega$ is the two-equation turbulence model based on the turbulent kinetic energy k and the specific dissipation ω. 13, 16

u' The root-mean-square turbulent velocity fluctuation. $u' = \sqrt{\frac{1}{3}u_i' \cdot u_i'}$ with unit in $\frac{m}{s}$. 15

u^+ The non dimensional velocity. $u^+ = \frac{u}{u_\tau}$. 6

u_τ is the friction velocity in $\frac{m}{s}$. $u_\tau = \sqrt{\frac{\tau_w}{\rho}}$. 6

y^+ The non dimensional distance to the wall. $y^+ = \frac{y u_\tau}{\nu}$. 6, 17

HEXPRESS is an unstructured full-hexahedral meshing tool developed by Numeca Int. 3, 23, 52

MATLAB is a environment for numerical computation, visualization, and programming. It is distributed by The MathWorks, Inc. 3

OpenFOAM stands for Open Source Field Operation and Manipulation. 1, 3, 16, 23, 52

ParaView is an open source data analysis and visualization application distributed by Kitware, Inc. 3

Chapter 1

Introduction

The study of the hydrodynamics started more than a century ago, but the development of the computational hydrodynamics is only extended to the last decades. The computational power and the numerical algorithms have improved, and nowadays the Computational Fluid Dynamics (CFD) is a key tool in many industries. There is a wide range of solvers, from potential flow based solvers up to Direct Numerical Simulation (DNS) based methods. The choice depends on the problem statement. This master thesis is a study in ship hydrodynamics with the help of OpenFOAM as CFD tool. The computation of the ship viscous resistance is computed with a Reynolds Averaged Navier-Stokes (RANS) solver. The RANS solvers are the state of the art in the external flow computations due to the high quality of the results compared to the computational effort.

The present work is a study of the viscous resistance of two hulls. The first hull is a well studied case of a tanker developed by Korean Maritime and Ocean Engineering Research Institute (MOERI), the KRISO Very Large Crude Carrier (KVLCC2). The second hull is a cruise-ferry vessel (which study is relevant for the Marine Technology unit in Aalto University). These two vessels have the hull forms in the opposite extremes of the block coefficient range. While the tanker has a large block coefficient, designed for low sailing speeds (15 kn), the cruise ferry will operate at large speeds (21 kn) and her hull form is slender, with low block coefficient.

1.1 Previous work

The resistance of a ship is an information difficult to measure. One of the best ways to predict the resistance is by model tests in a towing tank. In order to extrapolate the results of the model to the full size ship, the resistance of the hull is divided in two main components: one characterized by the viscous effects and the other one based on the free surface effects. It is reasonable to relate viscous effects to the Reynolds number Re and the free surface effects to the Froude number Fr. The viscous effects are evaluated with the skin friction coefficients C_f and C_F.

The first experiments conducted by William Froude were about relating the friction resistance of a flat plate with the main dimensions. Afterwards, some correlated friction lines were calculated by Hughes [13], Schoenherr [30] and others. These lines correlate the mean skin friction C_F to the Reynolds number Re. Later on, in 1957, during the 8$^{\text{th}}$ International Towing Tank Conference (ITTC), the towing tanks determined one single correlation line [26] to use in ship model testing. This line unifies the calculations on friction coefficient in the naval sector, but it only provides the mean value all along the surface.

The latest correlation curves used on the aeronautical sector are based on experiments with high Reynolds numbers (Re up to $1.3 \cdot 10^9$ [25]). The semiempirical method developed by Winter and Gaudet [34] is reliable up to $Re = 4.5 \cdot 10^8$, but this method takes into account the compressibility, as the Mach number goes up to $Ma = 2.8$. The latest friction lines have been developed with the use of CFD tools [7, 17].

This thesis is part of a research in the Marine Technology unit of the Applied mechanics department of Aalto University. It is intended to be a research deeply in the shear stresses inside the boundary layer around a ship hull. The use of CFD tools enable the study of the 3D effects on the boundary layer with precision. The distribution of the shear stresses along a curved hull cannot be measured experimentally due to the requirements of the measuring equipment.

This work is focused on investigate the distribution of shear stresses with a CFD solver. This information is necessary to know the origin of the friction resistance on hulls.

1.2 Problem statement

The analysis of shear stresses is performed on two hulls. The first hull, the KVLCC2 will be used to adjust the variables affecting the solution. This hull has been tested in several papers [12, 14] and workshops [20, 21]. The results of the tanker will be compared and used to set up the turbulence variables in the second hull, the cruise vessel.

Each geometry is meshed with HEXPRESS, then computed with OpenFOAM, an open source CFD software package and the post processing is performed with both ParaView and MATLAB.

1.2.1 Solver selection

The solver selected is `simpleFoam`. This solver does not compute the free surface, as for example `interFoam` does. The research on shear stresses is not much influenced by the free surface effects and the duration of the computations would become thirty times longer. It is also influenced by the experimental tests on the KVLCC2. This hull was only tested in a wind tunnel [32], which means that there is no free surface.

Chapter 2

Background

2.1 Turbulent boundary layer

The boundary layer is a consequence of the viscosity of a fluid passing by the surface of a solid. The transition from laminar flow to turbulent takes place with Reynolds numbers around $5 \cdot 10^5$ [33, page 436]. This means that the transition of the flow occurs in the first 2% of the length in a model case hull and 0.03% in a real scale ship. The study of the laminar boundary layer is not relevant since almost all the length is in turbulent flow.

2.1.1 The boundary layer of a smooth flat plate

The development of the boundary layer along a flat plate is used as a reference frame. The flat plate is considered smooth, infinitely wide and its thickness is depreciated. It is aligned with the flow. The compressibility of the fluid is depreciated since the Mach number (Ma) is very small The thermodynamic effects are also not considered.

$$Ma = \frac{U_0}{c} = \frac{O(10)}{O(1000)} = O(0.01) < 0.3 \tag{2.1}$$

With these assumptions, the system can be explained with two dimensions, where the origin is located in the leading edge of the plate, the x axis is oriented with the flow and the y axis is perpendicular to the plate. The velocity field of the flow is represented by the vector $\vec{v} = (u, v)$. The initial speed of the flow is U_0 in the x direction (see figure 2.1).

Because of the viscosity and the non-slip condition on the surface of the plate, the velocity changes from zero speed at the wall to the free

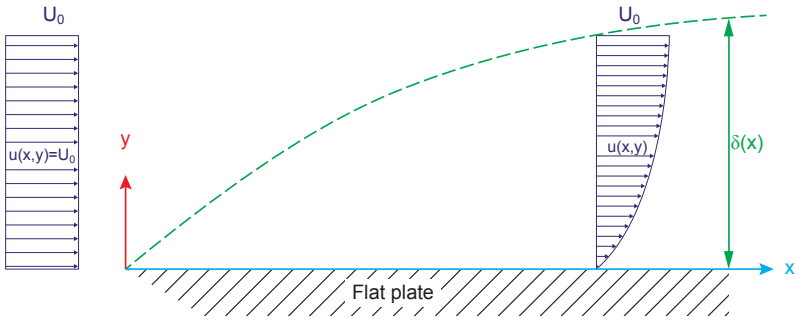

Figure 2.1: Reference sketch of the boundary layer on a flat plate.

stream velocity U_0 far from the wall. The *boundary layer* is the region where the speed is different than U_0. The *boundary layer thickness*, δ, is the distance in y directions where there is the frontier between the boundary layer and the free stream [29]. The definition of this thickness is:

$$\delta = y|_{u=0.995 \cdot U_0} \tag{2.2}$$

As this value may be difficult to estimate, the displacement thickness, δ^* and the momentum thickness, Θ, are introduced:

$$\delta^* = \int_0^\infty \left(1 - \frac{u}{U_0}\right) dy \tag{2.3}$$

$$\Theta = \int_0^\infty \frac{u}{U_0}\left(1 - \frac{u}{U_0}\right) dy \tag{2.4}$$

The value of the thickness is continuously increasing along x, based on the Reynolds number along the surface Re_x.

2.1.2 Morphology of the boundary layer

The experiments of Prandtl and von Kármán on the analysis of the boundary layer lead into three regions or layers [33]:

- The **inner layer** where the viscous effects dominate. It can be subdivided in two sublayers:
  - The **laminar or viscous sublayer**, next to the wall with no turbulent effects.

  - The **overlap or logarithmic sublayer** in between the inner and the outer, which has influence of both viscous and turbulent effects.

- The **outer layer** dominated by turbulent effects.

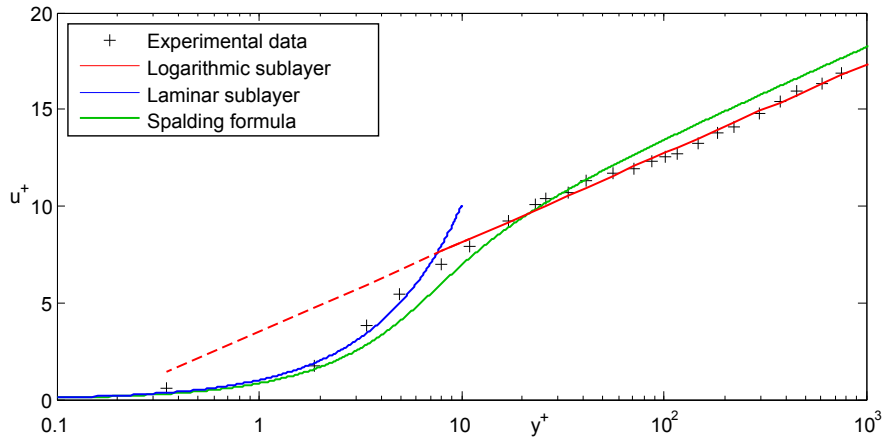

Figure 2.2: Morphology of the turbulent boundary layer. Source [9]

In the figure 2.2 it is possible to see the profile of the non dimensional velocities u^+, in function of the non dimensional distance to the wall y^+. The definitions of u^+ and y^+ are:

$$u^+ = \frac{\bar{u}}{u_\tau} \tag{2.5}$$

$$y^+ = \frac{y u_\tau}{\nu} \tag{2.6}$$

where u_τ is the friction velocity and ν is the viscosity of the fluid.

It is important to remark that the surface is considered smooth. The characteristics of the surface roughness have some impact on the extent of the outer layer [33, Ch.6].

2.1.2.1 Inner layer characteristics

The inner layer extends up to $y^+ \approx 350$. It is divided in two parts, the laminar sublayer and the logarithmic sublayer.

The laminar sublayer, also called viscous sublayer (as in 2.6.3 after [10]), extends from the wall to $y^+ \approx 5$. In this region the velocity profile is linearly proportional to the non-dimensional distance as it is in a laminar boundary layer.

$$u^+ = y^+ \tag{2.7}$$

The logarithmic sublayer goes from $y^+ \approx 35$ up to $y^+ \approx 350$. This upper limit is not completely fixed since it depends on the pressure gradient and the outer boundary layer. The name logarithmic layer comes from the defining formula.

$$u^+ = \frac{1}{\kappa} \ln y^+ + B \tag{2.8}$$

Where κ is the Kármán constant and B is the turbulent wall law intercept constant. Their values are $\kappa = 0.41$ and $B = 5.0$ from [4].

The region between $y^+ = 5$ and 35 (also called buffer sublayer) is neither linear nor logarithmic. A good approximation is the Spalding´s formula, which covers all the region up $y^+ > 300$.

$$y^+ = u^+ + e^{-\kappa B} \left[e^{-\kappa u^+} - 1 - \kappa u^+ - \frac{\left(\kappa u^+\right)^2}{2} - \frac{\left(\kappa u^+\right)^3}{6} \right] \tag{2.9}$$

2.1.2.2 Outer layer characteristics

This layer, also called *velocity-defect layer*, is explained as the deceleration of the flow. It is a function of the boundary shape $\left(\frac{y}{\delta}\right)$ and the pressure gradient ξ.

$$\frac{U_\infty - \bar{u}}{u_\tau} = \frac{-1}{\kappa} \ln \frac{y}{\delta} + A\left(\xi\right) \tag{2.10}$$

2.1.3 Effects of the curvature in the boundary layer

The boundary layer can be easily related to the free stream flow in the case of a flat plate. With non-flat surfaces, the flow has to adapt to the

direction of the wall, changing the velocities along the surface. This has some effect on the boundary layer. The non-dimensional form is not influenced, but in the flow velocity and the thickness, which can be translated into a change of the friction resistance.

2.1.3.1 Change of the boundary layer with transverse curvature

The main effect of the transverse curvature is to decrease the thickness of the boundary layer. The experimental results in [6] gave a relation between the boundary layer thickness (δ_2) and the transverse curvature (R_c).

$$\delta_2 = \frac{\delta_{\text{flat plate}}}{\sqrt{1 + \frac{\delta_2}{3 \cdot R_c}}} \tag{2.11}$$

As the boundary layer is thinner, the shear stresses increase. This way, the friction resistance increases. These results are confirmed in [18].

2.1.3.2 Pressure distribution with longitudinal curved boundary layer

In longitudinal curved bodies, the viscous resistance increases. Apart of the friction provoked by the shear stresses, there is one other component, the viscous pressure resistance C_{PV}.

A simple explanation of the longitudinal curvature effect is explained with a two dimensional body. The variation of the velocity around the hull can be seen from the potential flow solution in figure 2.3. The flow has a stagnation point in the fore and aft ends, but the velocity is higher all along the hull. D'Alembert's paradox can be seen in the potential flow case. The integral of the pressures all around the hull gives zero as result.

$$\oint_{hull} p\mathbf{n_x} dA = 0 \tag{2.12}$$

This situation changes when the friction is not neglected. The boundary layer is developed from the fore part of the hull and backwards. The figure 2.4 shows the differences in pressure between the potential flow

and the real flow.

$$\oint_{hull} p\mathbf{n}_\mathbf{x} dA \neq 0 \tag{2.13}$$

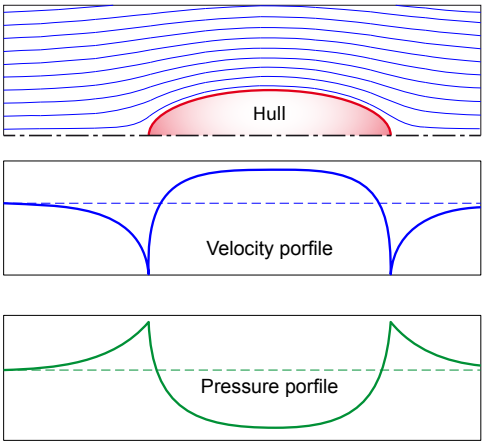

Figure 2.3: Potential flow around the hull.

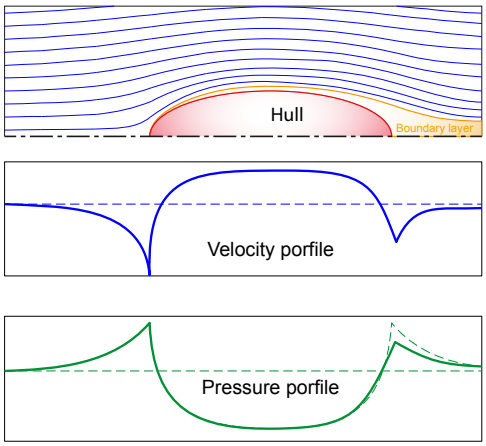

Figure 2.4: Flow around the hull with boundary layer.

2.2 The local skin friction coefficient C_f on a flat plate

The shear stresses in the flow are the result of the viscosity. These shear stresses are also appearing on the surface of a submerged solid and the effect is seen as frictional force F. In the case of a flat plate, the shear stresses on the wall τ_w are dependent on the fluid properties, viscosity ν and velocity U_0. The frictional force changes along the distance, x, from the leading edge and the shear stresses can be related with the surface of the plate A.

$$\tau_w(x) = \frac{dF}{dA} \quad \underset{plate}{\overset{flat}{\Longrightarrow}} \quad \tau_w(x) = \frac{dF(x)}{dxdz} \tag{2.14}$$

The local friction coefficient C_f is the non-dimensional expression of the local force, therefore it is also dependent on the distance x to the leading edge.

$$C_f(x) = \frac{dF}{\frac{1}{2}\rho U_0^2 dA} \tag{2.15}$$

Where ρ is the mass density of the fluid and U_0 is the free stream velocity. The equations 2.14 and 2.15 can be combined to obtain the relation between the local friction and the shear stress [1, page 14].

$$C_f(x) = \frac{\tau_w}{\frac{1}{2}\rho U_0^2} \tag{2.16}$$

2.2.1 Friction coefficient in laminar flow

The flow is laminar when the flow stays in different layers without lateral mixing [3]. The Reynolds number Re_x of a laminar flow along a flat plate is below $5 \cdot 10^6$. Around this point, the flow will start to become turbulent. For laminar flow, the local skin friction coefficient is obtained with the Blasius formula for laminar flow [33, formula 4-52].

$$C_f = \frac{0.664}{\sqrt{Re_x}} \tag{2.17}$$

where Re_x is the Reynolds number at the distance x from the leading edge.

2.2.2 Friction coefficient in turbulent flow

In the case the local Reynolds number is high (over the mentioned value of $5 \cdot 10^6$), the flow is turbulent. This turbulent transition can also be artificially created with i.e. excitation studs or surface roughness. At this point, the formula 2.17 is replaced by the formula obtained by Kestin and Persen [33, formula 6-78].

$$C_f \approx \frac{0.455}{\left(\ln\left(0.06 Re_x\right)\right)^2} \tag{2.18}$$

This explicit formula has an error of 1% in comparison to the implicit formula derived from Spaldingś wall formula 2.9. It is important to note that the turbulent flow is assumed to be turbulent from the leading edge ($x = 0$).

2.3 The mean skin friction coefficient C_F on a flat plate

The idea of evaluating the skin friction on a flat plate is to relate the drag to its main dimensions. Therefore, it has been more useful for the

naval industry to calculate the mean friction coefficient along all the plate. This is used to calculate the skin friction of a ship hull. The total frictional force is the integral of the local force on the surface S:

$$F = \int_S dF = \int_S \tau_w(x)\, dA \tag{2.19}$$

The mean skin friction coefficient C_F, is the non-dimensional form of the total force

$$C_F = \frac{F}{\frac{1}{2}\rho U_0^2 S} \tag{2.20}$$

Considering the surface of the flat plate as $S = b \cdot L$ and using formulas 2.16 and 2.19 in 2.20, the relation between the local and the mean friction coefficients is

$$C_F = \frac{\int_S \tau_w(x)\, dA}{\frac{1}{2}\rho U_0^2 S} = \frac{1}{L}\int_L C_f(x)\, dx \tag{2.21}$$

which is the definition of a mean value.

2.3.1 Mean skin friction coefficients of a flat plate

The integral form of the local coefficients has been calculated by the same authors as the local formulas. The mean friction coefficient in a laminar flow is the integral performed in 2.21 of the formula 2.17:

$$C_F = \frac{1}{L}\int_L \frac{0.664}{\sqrt{Re_x}}(x)\, dx = \frac{1.328}{\sqrt{Re_L}} \tag{2.22}$$

In the case of the turbulent flow, the mean friction coefficient of a flat plate is estimated as:

$$C_F \approx \frac{1}{L}\int_L \frac{0.455}{\left(\ln\left(0.06Re_x\right)\right)^2}(x)\, dx = \frac{0.523}{\left(\ln\left(0.06Re_L\right)\right)^2} \tag{2.23}$$

2.4 Friction line for ship correlation

As explained in the beginning of the chapter, the friction resistance of a ship is related to its Reynolds number. The idea of measuring the resistance of a ship using a scaled model has been performed since 19$^{\text{th}}$ century, when William Froude was predicting the resistance of a hull in Torquay [28]. As the tests are scaled using the same Froude number, the viscous effects are to be correlated from the model to the full scale.

2.4.1 Early correlation lines

Prior to 1957, each towing tank had its own correlation line. The most used ones were the curves fitted by Schoenherr [30] and Hughes [13]. The first one was mainly used by the American Towing Tank Conference (ATTC) tanks. The correlation is implicit:

$$\frac{0.242}{\sqrt{C_F}} = \log\left(Re_L \cdot C_F\right) \tag{2.24}$$

On the other hand, the experiments conducted with planks reaching Reynolds numbers around $Re_L = 3 \cdot 10^8$ were tested by Hughes to extrapolate a curve of minimum turbulent resistance. The use of this curve was more common in Europe, and the equation is

$$C_F = \frac{0.066}{\left(\log Re_L - 2.03\right)^2} \tag{2.25}$$

2.4.2 ITTC57 correlation line

In 1957, during the 8$^{\text{th}}$ ITTC, the towing tanks determined one single correlation line [26]. This curve had to be as steep as the Hughes' for low Reynolds number, but it had to increase the friction coefficient for high Reynolds values. The agreed formula, which will be used as a reference value in this thesis, is:

$$C_{F0}\left(ITTC57\right) = \frac{0.075}{\left(\log Re - 2\right)^2} \tag{2.26}$$

This correlation line is related to ship hulls, therefore, the values are higher if compared to a flat plate.

2.4.3 Hull form factor

The correlation of the different hulls with the ITTC57 friction line takes into account the effects of the friction resistance, but this does not mean that all the viscous effects are included. The viscous resistance C_V includes the friction resistance as well as the effects of the curvature and some other effects that affect the boundary layer, as it could be the separation, three dimensional effects or the transition from laminar to turbulent. The three dimensional effects can be explained as the integral of the momentum thickness (eq. 2.3) on the hull [33].

These effects have been grouped in the form factor coefficient k. This factor represents the increase of the viscous resistance related to the equivalent flat plate [27].

$$C_{viscous} = C_F + C_{PV} = (1 + k) \cdot C_{F0} \tag{2.27}$$

where C_F is the friction coefficient from formula 2.20, C_{PV} is the viscous pressure resistance coefficient and k is the form factor.

2.5 The frame skin friction coefficient $\breve{C}_f$

The skin friction resistance has been related to flat plates. The first implicit assumption is that the friction is not dependant on the z-direction. This means the shear stresses are the same in the upper edge of the plate than the stresses in the middle or in the bottom. The assumption is close to the reality since the flow is almost the same at these different depths. The problem appears in the study of hulls with double curvature. In order to evaluate the friction effects along a curved hull, the new concept of *frame skin friction coefficient* $\breve{C}_f$ is introduced as the average friction coefficient along a frame of length L_{frame}.

$$\breve{C}_f(x) = \frac{\int_{L_{frame}} \tau_w(x, s)\, ds}{\frac{1}{2}\rho U_0^2 L_{frame}} \tag{2.28}$$

A similar approach can be performed with the viscous pressure distribution $\breve{C}_{PV}$.

$$\breve{C}_{PV}(x) = \frac{\int_{L_{frame}} p \cdot \mathbf{n_x}(x, s)\, ds}{\frac{1}{2}\rho U_0^2 L_{frame}} \tag{2.29}$$

2.6 Turbulence model $k - \omega$

The $k - \omega$ turbulence model is the most extended model in the study of flows around ships. This model is the evolution of the $k-\epsilon$ developed by Menter [23] and the variant used is the Shear Stresses Transport (SST) model. The model is defined with two equations, one equation for the turbulent energy k and the second equation for the specific dissipation of turbulent kinetic energy ω.

2.6.1 Theoretical approach

The transport equations of these two variables are now described. The equation of the turbulent energy k is:

$$\frac{\partial \rho k}{\partial t} + \frac{\partial \rho \bar{u}_i k}{\partial x_i} - \frac{\partial}{\partial x_i}\left[(\mu + \sigma_k \mu_t)\frac{\partial k}{\partial x_i}\right] = \tau_{ij}\frac{\partial \bar{u}_i}{\partial x_j} - \beta^* \rho k \omega \tag{2.30}$$

And the second equation for the specific dissipation ω:

$$\frac{\partial \rho \omega}{\partial t} + \frac{\partial \rho \bar{u}_i \omega}{\partial x_i} - \frac{\partial}{\partial x_i}\left[(\mu + \sigma_k \mu_t)\frac{\partial \omega}{\partial x_i}\right] = \frac{\gamma}{\nu_t}\tau_{ij}\frac{\partial \bar{u}_i}{\partial x_j} - \beta^* \rho \omega^2 \tag{2.31}$$

There are different versions of the $k-\omega$ model. All of them are based on the same transport equations with different definitions of the constants included. The SST model is the only one used in this research. This model has the benefit of blend to a $k-\epsilon$ model in the flow free of shear stresses. The blend is based on two functions F_i of the distance y to the nearest wall.

$$F_1 = \tanh\left(arg_1^4\right) \tag{2.32}$$

$$arg_1 = min\left(\frac{4\rho k \sigma_{\omega 2}}{CD_{k\omega} y^2}; max\left(\frac{\sqrt{k}}{0.09\omega y}; \frac{500\nu}{\omega y^2}\right)\right) \tag{2.33}$$

$$CD_{k\omega} = max\left(2\rho\frac{\sigma_{\omega 2}}{\omega}\frac{\partial k}{\partial x_i}\frac{\partial \omega}{\partial x_i}; 10^{-20}\right) \tag{2.34}$$

The second blending function is:

$$F_2 = \tanh\left(arg_2^2\right) \tag{2.35}$$

$$arg_2 = max\left(\frac{2\sqrt{k}}{0.09\omega y}; \frac{500\nu}{\omega y^2}\right) \tag{2.36}$$

Both blending functions are zero in the field and the value turns gradually to one while approximating to the wall 2.5.

The constants listed change the value from the inner region to the outer region with the values of this region (see table 2.1).

This way, the values of the variables blend between regions by weighting the two values with the function F_1 as it does with β in 2.6.1.

$$\beta = F_1 \cdot \beta_1 + (1 - F_1) \cdot \beta_2 \tag{2.37}$$

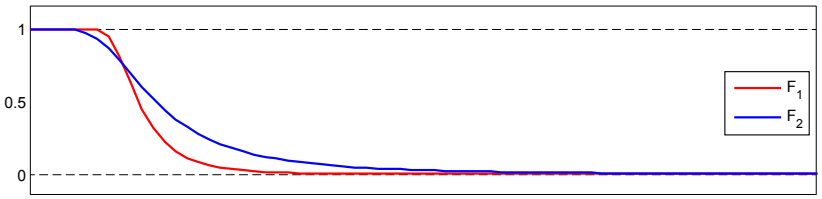

Figure 2.5: Behavior of blending functions of SST.

Inner region	$\beta_1 = 0.075$	$\beta^* = 0.09$	$\gamma_1 = 0.567$
	$\sigma_{k1} = 0.850$	$\sigma_{\omega 1} = 0.500$	
Outer region	$\beta_2 = 0.0828$	$\beta^* = 0.09$	$\gamma_2 = 0.463$
	$\sigma_{k2} = 1.000$	$\sigma_{\omega 2} = 0.856$	

Table 2.1: Constants of the $k - \omega$ model

Except for ν_t which changes with F_2:

$$\nu_t = \frac{0.31k}{max\left(0.31\omega; F_2\Omega\right)} \tag{2.38}$$

2.6.2 Practical approach

The values of the two variables k and ω are related to the ship dimensions. In the case of the kinetic energy, it is more common to provide the turbulence intensity, I, since it is a non dimensional value given as a percentage.

$$I = \frac{u'}{U_0} = \frac{\sqrt{\frac{1}{3}u_i' \cdot u_i'}}{U_0} \tag{2.39}$$

$$k = \frac{3}{2}\left(I \cdot U_0\right)^2 \tag{2.40}$$

Where U_0 is the reference speed of the vessel and u' is the mean fluctuation of the velocity.

The range of values of the turbulence intensity in the flow around a vessel is $I \in (2\% - 4\%)$. In the figure 2.6 it is possible to see the variance of the results in this range.

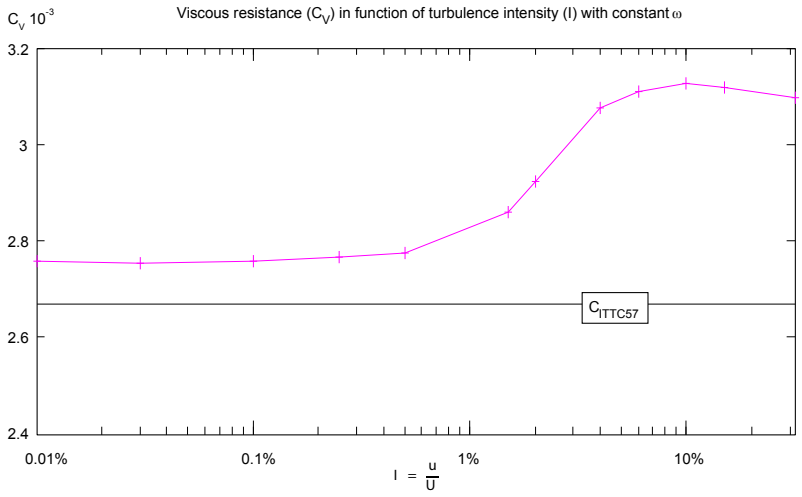

Figure 2.6: Influence on the viscous resistance C_V of the turbulence intensity I.

There is no strict mathematical definition of the specific turbulence dissipation ω, but the numerical experiments on flat plates suggest the following value [7]:

$$\omega = 10\frac{U_0}{L} \tag{2.41}$$

As the friction lines are referred to the length L, it is normal to use the length of the hull, L_{PP} as reference value.

2.6.3 Wall functions

The behavior of the boundary layer can be predicted as it is explained in 2.1. It would be wise to implement a *wall function* which emulates the behavior of the flow inside the boundary layer. As the flow is easier to calculate in this region, no grid refinement is necessary inside the region nor computation of the equations required. This way, the wall function reduces the numerical effort [8]. The wall function is connected to the turbulence model, in this case $k-\omega$ SST. In the case of OpenFOAM, there are wall functions for k, ω and ν_T [24].

The transport equations of functions are based on the notation of the figure 2.7, where the coordinate system is represented. The variable y is again the distance to the wall. Note that the scale of this

distance y is smaller than the scale of the blend functions 2.6.1 and 2.6.1, but the concept is same [10].

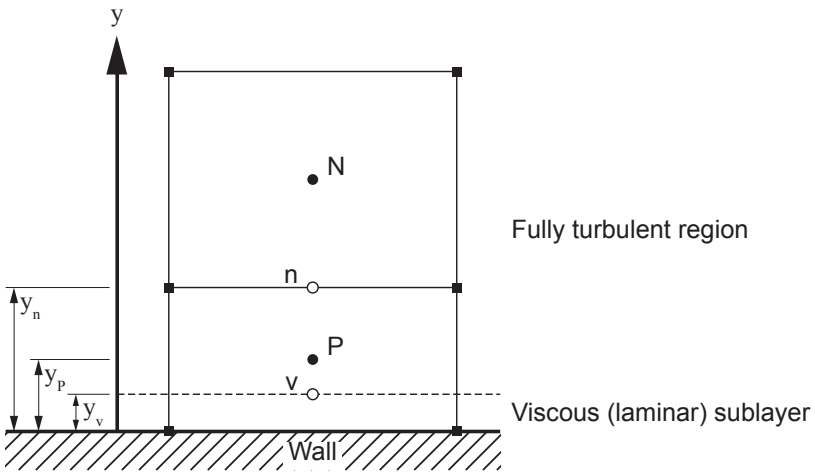

Figure 2.7: Cell notation by the wall functions.

The value y_v is the distance from the wall to the laminar (viscous) sublayer. This distance varies along the hull, but the y^+ value is constant. In the general equations it is equal to $y_v^+ = 11.6$ [10], but in the implementation in OpenFOAM this value is 11.0. This distance is used to create the ghost node v in which the kinetic energy k is evaluated (k_v). The value k_v is used to calculate a zero gradient in the normal direction $\left(\frac{\partial k}{\partial n} = 0\right)$, and the value on the centroid of the cell is calculated as:

$$k_P = \frac{u_\tau^2}{y_P \sqrt{C_\mu}} \tag{2.42}$$

The friction velocity u_τ is calculated with the automatic blending function:

$$u_\tau^{lam} = \frac{U}{y_n^+} \qquad\qquad u_\tau^{log} = \frac{U}{\log E y_n^+} \tag{2.43}$$

$$u_\tau = \sqrt[4]{(u_\tau^{lam})^4 + \left(u_\tau^{log}\right)^4} \tag{2.44}$$

Where E is a constant equal to 9.8.

The 4$^{\text{th}}$ power blends the function to laminar in the cases where y_n^+ is small and to logarithmic for large values. y_n^+ is evaluated with the cell height y_n, velocity u_n and fluid viscosity ν.

$$y_n^+ = \frac{y_n \cdot u_n}{\nu} \tag{2.45}$$

These previous equations are also valid in a $k-\epsilon$ turbulence model. The dissipation of turbulent kinetic energy ω is also blended, in this case with a 2$^{\text{nd}}$ power distance [22]:

$$\omega_{lam} = \frac{6\nu}{\beta y_P^2} \qquad\qquad \omega_{log} = \frac{u_\tau}{\sqrt[4]{C_\mu}\kappa y_P} \tag{2.46}$$

$$\omega_P = \sqrt{(\omega_{lam})^2 + (\omega_{log})^2} \tag{2.47}$$

Where the constants are: β equal to 0.075, C_μ 0.09 and κ 0.41 (von Kármán's constant). The distance to the wall y_P in this case is measured to the centroid of the cell.

Chapter 3

Hulls

This thesis investigates two hulls, one of a tanker, the KVLCC2 and the second one of a cruise ferry. The first one will be used both for validation and analysis, while the cruise will be used only for analysis.

3.1 KVLCC2

The KVLCC2 is the second version of a tanker designed in Korean Institute of Ships and Ocean Engineering. (KRISO) (it changed its name to MOERI) [19]. This tanker was designed to provide data from a wind-tunnel in order to validate the CFD flow around the hull. This data will be used to validate the results of the model scale. As it is a validation case, this hull has been studied in deep. The results of the Gothengburg 2000 workshop [20] will be used to set up the conditions. The full-scale ship was never built.

This hull of a modern tanker has bulb both in the bow and astern. She has a large block coefficient (C_B). The rest of the geometry conditions are showed in table 3.1, and the lines are plotted in 3.1.

Size Scale	Full scale 1.0	Model scale 1 : 58.0
Main particulars		
$L_{WL}(m)$	325.5	5.6121
$B_{WL}(m)$	58.0	1.0000
$T(m)$	20.8	0.3586
$\nabla(m^3)$	312622	1.6023
$S(m^2)$	27194	8.0838
C_B	0.8098	0.8098
C_M	0.9980	0.9980
Test conditions		
U_0	15.5 **kn**	1.047 $\left(\frac{m}{s}\right)$
Re	$2.03 \cdot 10^9$	$4.6 \cdot 10^6$

Table 3.1: Geometry and conditions of the KVLCC2 case.

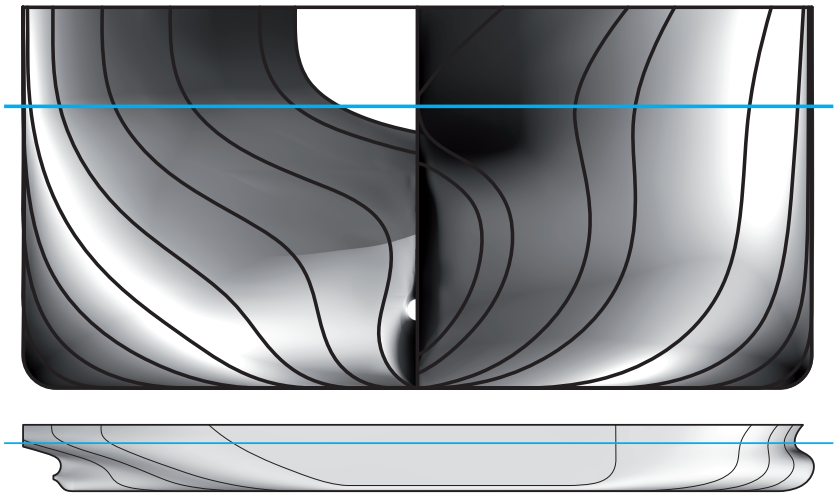

Figure 3.1: Hull drawings of the KVLCC2 from the geometry file [19]. The water line is in blue.

3.2 Cruise ferry case

The cruise ferry hull has been selected because it is a case opposite of a tanker. She has a slender hull and higher design speed. The ship has been built, but the performance data for the case without free surface is not available.

The hull has a pierced bulbous bow designed for her speed. The stern of the hull maintains almost constant breadth and she has a centerline skeg. This hull is provided by STX Finland. The geometry conditions are in table 3.2, and the lines are plotted in 3.2.

Size Scale	Full scale 1.0	Model scale 1 : 22.713
Main particulars		
$L = L_{PP}(m)$	200.8	8.8496
$L_{WL}(m)$	204.8	9.0190
$B_{WL}(m)$	35.0	1.5410
$T(m)$	6.8	0.2994
$S(m^2)$	7815.4	15.1497
C_M	0.9821	0.9821
Test conditions		
U_0	21.0 **kn**	2.2668 $\left(\frac{m}{s}\right)$
Re	$2.21 \cdot 10^9$	$20.06 \cdot 10^6$

Table 3.2: Geometry and conditions of the cruise ferry case.

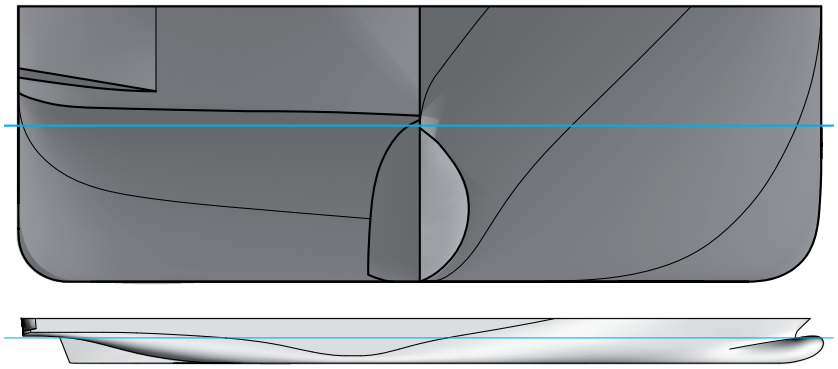

Figure 3.2: Hull concept drawings of the cruise ferry. The water line is in blue.

Chapter 4

Implementation

The use of CFD tools require some steps to preprocess the problem. The domain is meshed from the geometry of the hull. Once the grid is created, the boundary conditions are imposed an the computation begins.

The flow computation is set up firs for the KVLCC2. The results will be compared to the values of The Workshop of Gothenburg 2000 [20]. This is to check the turbulence variables have the correct values. Afterwards, in order to validate the results, there is a comparison with the experimental data from the wind tunnel [15].

Once the settings are validated, the shear stresses are analyzed in the two vessels in both model and full scale.

4.1 Grid generation from the geometry

The geometries of the hulls presented in chapter 3 are provided as surface files, in this case IGES format [2]. The geometry is composed of several patches, which are NURBS surfaces. There is a minor work checking these IGES files due to connectivity failures, precision errors or missing surfaces (i.e. the transom). Once the geometry file is *clean*, it can be imported in the grid generation software.

The hulls are defined following the recommendations of ITTC [1]. The main dimension of the ship, the length L_{PP}, is aligned with the X-axis. The aft perpendicular is located at $x = 0$ and the fore perpendicular is in positive values. The Y-axis is defined positive towards port side of the hull and the vertical axis z is positive upwards.

4.1.1 OpenFOAM tools: blockMesh and sHM

The process of meshing on OpenFOAM is done in two steps. In first place, a structured domain is created with *BlockMesh*. Afterwards the snap tool of OpenFOAM, *snappyHexMesh*, refines the mesh, snaps the geometry and creates the grid of the boundary layer. This last point was not possible to perform since the geometry of the hull seems to be too complex for *snappyHexMesh*. SnappyHexMesh generates a 3D meshes from triangulated surface geometries in Stereolithography (STL) format. After an exhaustive research on the tool, it was discarded since it cannot generate grids with the required quality for this thesis. The main problem was the lack of boundary layer grid.

4.1.2 HexPress

HEXPRESS is an unstructured full-hexahedral meshing tool. The mesh grid is created from a 3D solid model in Parasolid format [31], therefore, the IGES format is to be converted into Parasolid format with a CAD software. Once the domain is defined, Hexpresss creates a triangular mesh in order to generate the grid. The grid is generated in five steps: initial mesh, adaptation to the geometry, snap to geometry, optimize mesh and viscous layer addition. The last task after the mesh is created, is to export it to OpenFOAM. The `boundary` file is to be corrected by changing the mirror patches to `symmetryPlane`.

4.2 Dimensions of the domain

The grid is created following the recommendations of the ITTC [16]. The reference dimension is the length between perpendiculars, L_{PP}. Based on this value, the reference dimensions of the domain are listed in table 4.1. Afterwards, the exact value is rounded to the closest integer in order to simplify the calculations. A sketch can be seen in figure 4.1.

Direction	minimum value	maximum value
X	-3 to $-4 \cdot L_{PP}$	2 to $2.5 \cdot L_{PP}$
Y	0 (symmetry condition)	1 to $1.5 \cdot L_{PP}$
Z	$-1 \cdot L_{PP}$	0 (no free surface)

Table 4.1: Domain dimensions.

The problem is categorized as quasi-steady (or pseudo-transient, meaning the same). It means that the solution remains steady after certain time lapse. For this specific problem, the time lapse or time of simulation is $T_{sim} \approx 5\frac{L}{U_0}$ which means 20 seconds of simulation for model scale and 100 seconds for full scale. The time step is recommended to be $\Delta t = 0.001\frac{L}{U_0}$ as in [16, page 11]. The value is also to be checked with the Courant number Co so it is below 1 as a convergence prerequisite [5].

$$Co = \frac{u\Delta t}{\Delta x} < 1 \tag{4.1}$$

4.3 Boundary conditions

The boundaries are implemented on the external faces of the domain or *patches*. Both hulls have the same patch nomenclature, explained with the figure 4.1 and the table 4.2.

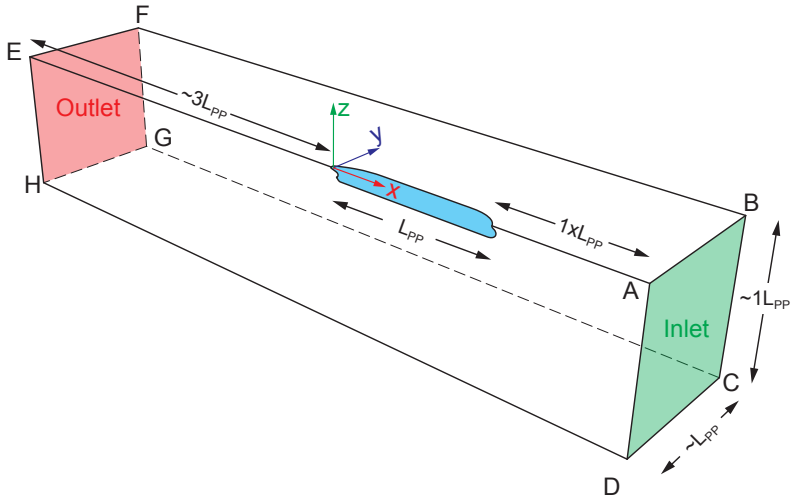

Figure 4.1: Domain patches and main dimensions.

The *fixed values* of table 4.2 are:

- Reference pressure $p_\infty = 0$. The value is set up to zero because it only works as a reference pressure.

	p	U	k	ω	Corners	Patch name
Inlet	zero grad.	fixed value			ABCD	inlet_w
Outlet	$p = p_\infty$	zero gradient			EFGH	outlet
Ceiling	slip condition				ABFE	ceiling_a
Port side	slip condition				BCGF	portside_w
Bottom	zero gradient				CDGH	bottom_a
Center plane	symmetry condition				ADHE	crujia
Hull patches	zero grad.	$\mathbf{U} = \bar{0}$	Wall functions		ADHE	hull_surface.*
Internal field	fixed value				Initial value	

Table 4.2: Boundary conditions and domain initial value.

- The inlet velocity has the direction $(-1, 0, 0)$ due to the frame of reference selected 4.1. The magnitude of the vector is the reference velocity U_0, selected from tables 3.1 and 3.2.
- The turbulent kinetic energy is evaluated from the turbulence intensity formula 2.6.2. As it is demonstrated in chapter 5, the turbulence intensity is chosen as $I = 3.5\%$.
- The specific dissipation of turbulent kinetic energy is chosen as $\omega = 10 \cdot \frac{U_0}{L_{PP}}$

The boundary conditions in OpenFOAM can be divided as primitive types and derived types [24, page U-133].

- *Fixed values*. This one corresponds to Dirichlet condition.
- *Zero gradient*. This one corresponds to Neumann condition in every dimension.
- *Slip condition*. If the variable is scalar (p or k), this condition means *Zero gradient*. For a vector, the normal component is *fixed value* zero, and the tangential components are *zero gradient*.
- *Symmetry condition*. This condition is implemented as a base type. The behaviour is similar to the *slip condition*.
- Wall functions. Applied on k and ω the function is described in section 2.6.3. The values used with these functions are: $k = 0$ and $\omega = 10 \cdot \frac{U_0}{L_{PP}}$.

The implementation of the boundary conditions in OpenFOAM is given as example in the appendix A

4.4 Shear stresses analysis

The distribution of shear stresses is analyzed along the hull. As the information of shear stresses τ_W is available for the whole surface, the component in the x direction τ_x is plotted as contour plots (iso curves). In order to compare with the friction curves (described in chapter 2), the shear distribution of different water lines and longitudinal cuts are plotted as function of the x position.

4.4.1 The frame skin friction coefficient

The velocities *near* the surface are influenced by the curvature of the surface and some other parameters. Therefore, the development of the 2D boundary layer along a flat plate cannot be applied to the hull surface. One of the solutions is to take longitudinal cuts as just described. But this solution does not take into account the development of the flow in the perpendicular direction to the cutting plane, i.e.: the vertical flow is not represented on the water line distribution. Other option is to follow a stream line on the hull surface, but as the non-slip condition has been applied on this surface, the velocity is zero.

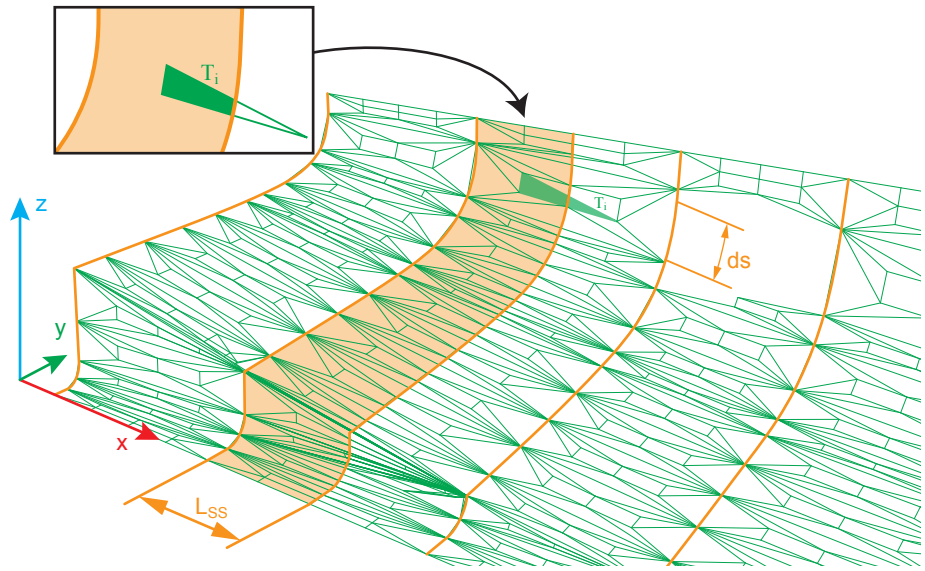

Figure 4.2: Sketch of the frame strip integration.

In order to obtain a representative value of the longitudinal shear

stress, the friction coefficient is averaged along a station, as explained in formula 2.28.

Since the domain has been discretized in cells, the value is averaged in strips defined by stations (see figure 4.2). The formula 2.28 can be expressed as

$$\breve{C}_f(x) = \frac{\int_{L_{frame}} \tau_x(x,s)\, ds}{\frac{1}{2}\rho U_0^2 L_{frame}} \approx \frac{\int_x^{x+L_{SS}} \int_{L_{frame}} \tau_w(x,s)\, dsdx}{\frac{1}{2}\rho U_0^2 \int_x^{x+L_{SS}} \int_{L_{frame}} dsdx} \tag{4.2}$$

where L_F is the perimeter length of the frame at position x. ds is the differential length of a curve on the station. L_{SS} is the length of station spacing.

The discrete surface is decomposed to triangles. Only the region of the triangle T_i inside the strip is added to the strip integral as seen in the detail of the figure 4.2. The integral of the shear stress in each triangle is linear evaluated on its barycenter. By definition, this is equivalent to the mean value of the vertices of the triangle.

Chapter 5

Results on KVLCC2

The reference hull, the KVLCC2 is computed to validate the results.

5.1 Influence of the turbulent quantities on the result

The turbulence quantities k and ω have a big influence on the results of the viscous resistance computation. In order to validate the initial values, the KVLCC2 case has been compute with a wide range of values, with special refinement around the recommended range $I \in (2\% - 4\%)$. The kinetic energy k is calculated from the turbulence intensity with formula 2.6.2. The computed values are:

$$I = \begin{bmatrix} 10^{-2} & 10^{-1.5} & 10^{-1} & 10^{-0.5} & 0.5 & 1.0 & 1.5 & 2.0 \\ 2.5 & 3.0 & 3.5 & 4.0 & 4.5 & 5.0 & 7.5 & 10 \end{bmatrix} \% \tag{5.1}$$

The values of the turbulence dissipation ω have been chosen to cover values of different order of magnitude. Nevertheless, the recommended value for flat plates 2.6.2. This formula with the conditions of the KVLCC2 listed in 3.1 result as:

$$\omega_{KVLCC2} = 10\frac{1.047}{5.5172} = 1.8977 s^{-1} \tag{5.2}$$

The computed values of the dissipation are:

$$\omega = \left[10^{-3}; 10^{-2}; 10^{-1}; 1; 2; 10; 10^{2}\right] s^{-1} \tag{5.3}$$

5.1.1 Meshed grid on the KVLCC2 model scale

The grid is meshed with Numeca HexPress. This mesher creates a initial block of cubic cells filling the domain. In the case of the KVLCC2 the initial size is 0.25 m. This cells are refined next to the selected surfaces, in this case the hull, or in volumes, for example a cylinder around the location of the propeller. The refinement consists in a division of the cubic cells in eight parts (2^3). As the refinement applied on this case is 5 levels, the average size of the cells next to the hull is:

$$\Delta x_N = \frac{\Delta x_0}{2^N} = \frac{0.25m}{2^5} = 7.8125mm \tag{5.4}$$

After the refinement, the cells are snapped by the hull surface. The grid is adapted to the hull and the domain. Once the cells are snapped, this program optimizes the geometry of the cells in order to have a better shape of all the cells. The performance of the CFD solver is enhanced when the cells have a good geometry (size and ratios, skewness, cell-faces...).

The last step is the addition of the boundary layer grid. The grid next to the hull surface will have the solution of the fluid in the boundary layer. The velocities are mainly parallel to the surface. Therefore, it is required to have a grid with one direction perpendicular to the surface and the other two parallel. This grid has a first layer next to the wall with a value of y^+ around 60. This value is set as input in HexPress obtaining a cell height of $2mm$. This height is calculated by a internal function based on the Reynolds number [11]. The expansion ratio is chosen with the first and latest cells heights and the number of layers, in this case $N = 10$.

$$r = \left(\frac{\Delta x_N}{\Delta y_1}\right)^{\frac{1}{N}} = \left(\frac{7.8125mm}{2mm}\right)^{\frac{1}{10}} = 1.146 \tag{5.5}$$

The map of the computations is plotted on figure 5.1 from the values of table 5.1.

The viscous resistance remains practically invariant for turbulence intensities below 1%. On the other hand, the resistance escalates rapidly if the intensity is higher than 5% and the dissipation is small.

Turbulence Intensity I(%)	Turbulent dissipation $\omega\,(s^{-}1)$						
	10^{-3}	10^{-2}	10^{-1}	1	2	10	100
0.010	3.902	3.902	3.902	3.902	3.913	3.902	3.902
0.032	3.902	3.902	3.902	3.902	3.913	3.902	3.902
0.10	3.903	3.903	3.903	3.903	3.914	3.902	3.902
0.32	3.908	3.909	3.909	3.908	3.920	3.903	3.902
0.50	3.915	3.917	3.916	3.913	3.926	3.906	3.902
1.0	3.960	3.957	3.948	3.932	3.946	3.912	3.903
1.5	4.037	4.028	4.006	3.960	3.977	3.920	3.905
2.0	4.146	4.136	4.094	4.002	4.021	3.929	3.907
2.5	4.282	4.272	4.205	4.057	4.080	3.939	3.909
3.0	4.383	4.446	4.351	4.133	4.158	3.950	3.912
3.5	5.147	4.655	4.526	4.225	4.258	3.964	3.914
4.0	5.349	4.878	4.707	4.335	4.374	3.979	3.916
4.5	5.375	5.092	4.888	4.449	4.483	3.997	3.919
5.0	6.683	5.320	5.071	4.554	4.583	4.018	3.922
7.5	8.279	6.620	6.207	5.102	5.134	4.168	3.936
10	10.914	8.072	7.686	5.793	5.833	4.387	3.954

Table 5.1: Values of $C_V \cdot 10^3$ in the $\omega - I$ map

5.1.2 Comparison with the computed values on G2000

The Gothengburg 2000 Workshop on Numerical Ship Hydrodynamics [20] (G2000) is a reference of the state of art on CFD and it is used in this thesis to select the proper values of turbulence. The KVLCC2 case was computed with different approaches and codes. The mean value and standard deviation of the viscous resistance obtained on the workshop is $C_V = (4.308 \pm 0.226) \cdot 10^{-3}$. The data of the table 5.1 is compared to this value in order to see the *map of good approximations*. With this map of figure 5.2, it is possible to see that the recommended values of I and ω fit with the expected results.

Therefore, these values of the turbulent quantities will be used for all the cases.

$$\omega = 10\frac{U_0}{L_{PP}} \qquad\qquad I = 3.5\% \tag{5.6}$$

The selected values for the KVLCC2 cases are listed on table 5.2.

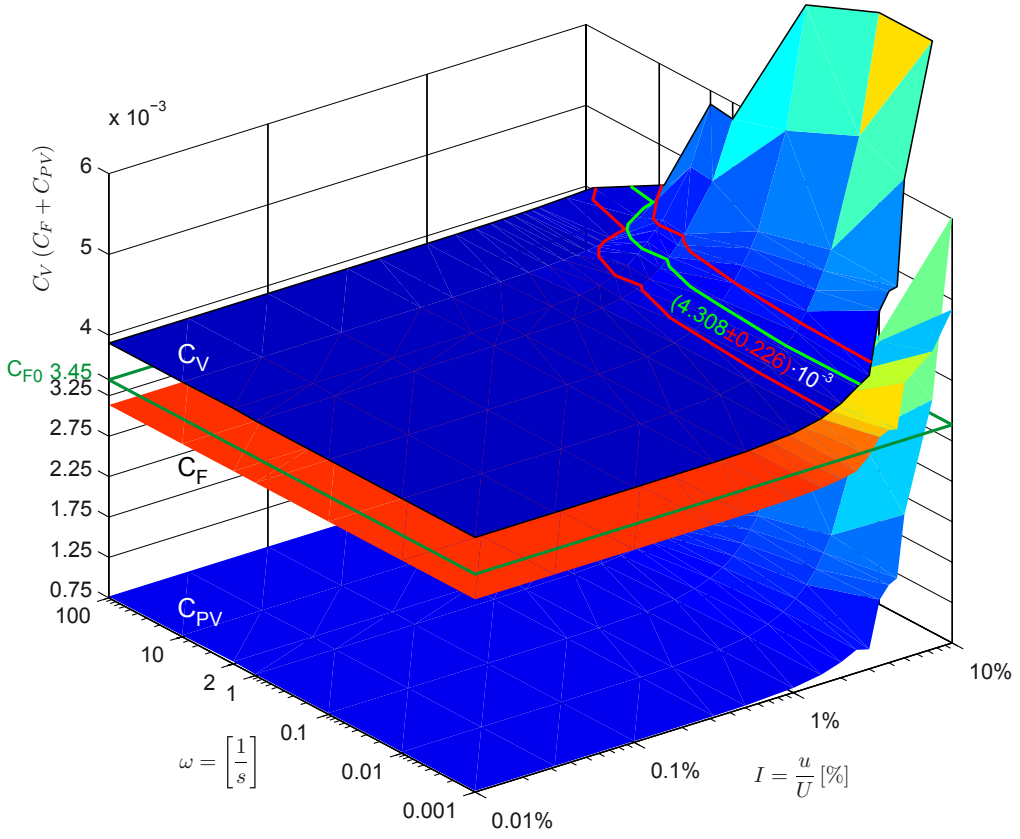

Figure 5.1: Influence of the initial values of I and ω on the viscous resistance.

Size	Full scale	Model scale
Scale	1.0	$1:58.0$
$L_{WL}(m)$	325.5	5.6121
Test conditions		
$U_0\left(\frac{m}{s}\right)$	7.974	1.047
Re	$2.03 \cdot 10^9$	$4.6 \cdot 10^6$
I	3.5%	
$k\,(m^2 s^{-2})$	0.1168	$2.0143 \cdot 10^{-3}$
$\omega\,(s^{-1})$	0.2492	1.8977

Table 5.2: Flow conditions of the KVLCC2 case.

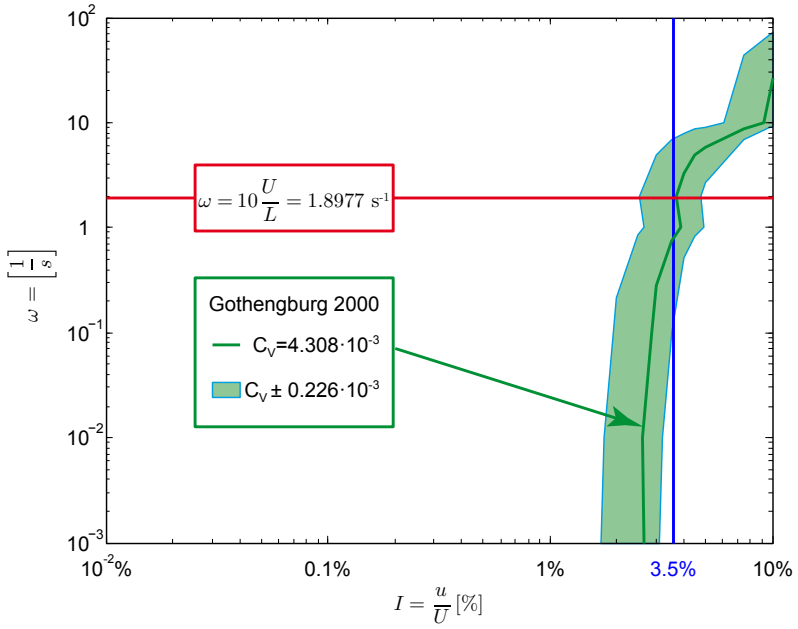

Figure 5.2: Comparison of viscous resistance values as function of I and ω with the results of G2000. The middle green line corresponds to the mean value of C_T and the green area is within one standard deviation.

5.2 Validation of the results with the experimental data

The experimental data obtained from the wind tunnel [19] is used to validate the results. The variables are measured at the propeller plane ($x = 0.0175 \cdot L_{PP} = 96.5mm$ from AP). The same conditions (table 3.1) are applied in the CFD model (with $\omega = 1.8977s^{-1}$ and $I = 3.5\%$). The grid has $1.65 \cdot 10^6$ cells.

5.2.1 Turbulent kinetic energy at the propeller plane

The kinetic energy of the turbulence is compared to the computed results. The contours in figure 5.3 show that the kinetic energy has the same order of magnitude. The resolution of the grid does not permit a better definition of the *hook-shaped* eddy formed from the skeg.

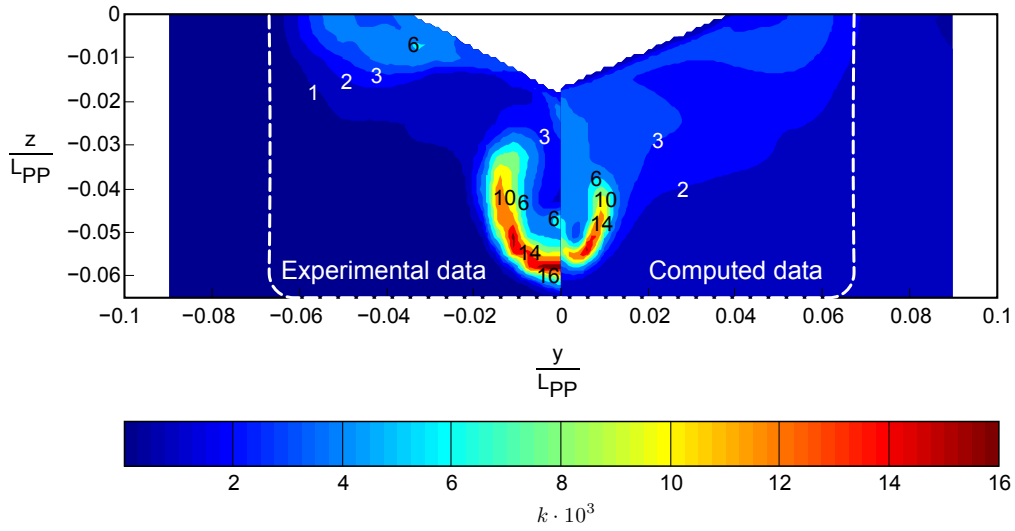

Figure 5.3: Comparison of the turbulent kinetic energy at the propeller plane of the experimental data (left) and the computed data (right).

5.2.2 Wake field at the propeller plane

The wake field plotted in figure 5.4 shows that the range of velocities is in the same range for both live test and the computation. The direction components form the same pattern. Once again, the computed solution cannot show the hook shaped profile of the skeg. The boundary layer is thicker in the computed data than the measured test.

5.2.3 Conclusions on the validation

The comparison of the calculated values shows a good correlation with the experimental data. The quality of the results is high if compared to the overall view. On the other hand, the correlation could be improved with a finer mesh, but this solution is out of scope due to the limitations of the present computers.

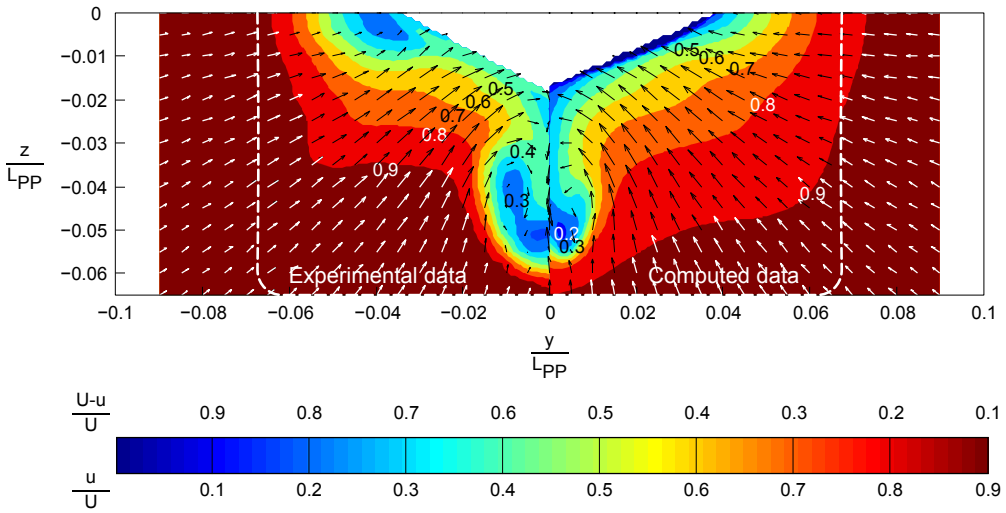

Figure 5.4: Comparison of the wake field of the experimental data (left) and the computed data (right).

5.3 Shear stress distribution in model scale

The distribution of shear stress in model is divided into three regions: the entry body, the parallel middle body and the run body. With this division, the plot of figure 5.5 with the friction coefficient distribution is analyzed.

The flow gets momentum in the entry body region, therefore the friction coefficient C_f is higher specially on the fore shoulder. Due to the stagnation on the upper part of the bulbous bow, the velocities on this part are small so is the friction coefficient. The parallel middle body shows almost constant friction coefficient. The evolution of the boundary layer is similar to a flat plate. There is a small increase of the friction on the bilge due to the transverse curvature effects explained with equation 2.1.3.1. The run body is immersed in a flow that has exchanged the momentum with the hull. The friction is lower in this region. Along the keel, specially the part on the skeg, the flow has a vertical component. This flow has not been slow down in the boundary layer, but comes from outside. Therefore, the shear stresses are higher on the keel.

The cuts of the hull show the shear stresses compared to the friction line by Kestin and Persen for turbulent flow 2.18. The figure 5.6 plots the friction coefficient along longitudinal cuts. The longitudinal

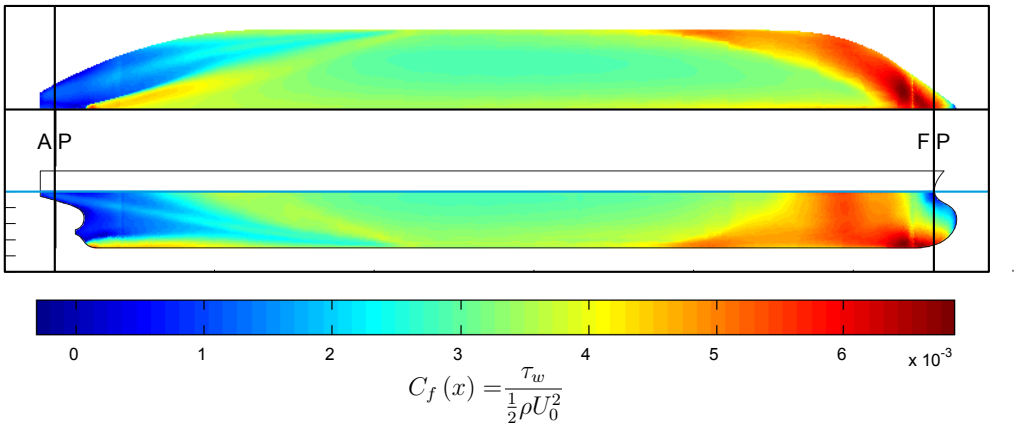

Figure 5.5: Friction coefficient distribution on the surface of the **KVLCC2 in model** scale.

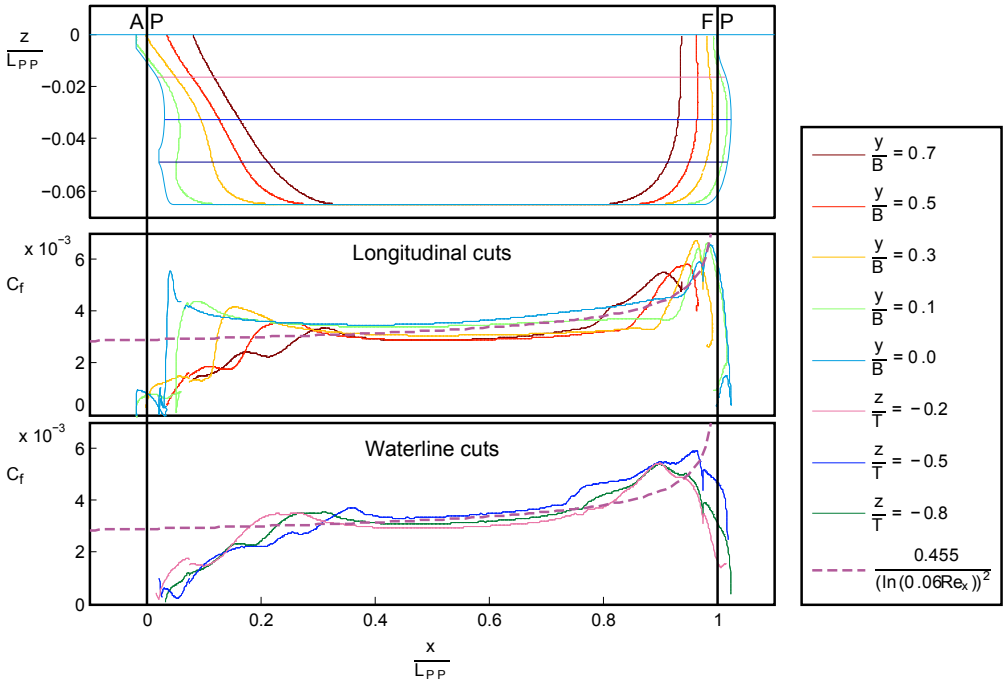

Figure 5.6: Friction coefficient distribution along water lines and longitudinal cuts of the **KVLCC2 in model** scale.

cuts (constant y) show the peaks on the friction coefficient on both the entry and the run bodies. The closer to the center line (keel) the more pronounced the peaks are. Furthermore, the stresses reveal a big peak on the skeg due to the incoming flow. The correlation of the calculated values with the friction line is better on the parallel middle body. This is confirmed with the water line cuts. The friction coefficient on the upper water lines is longer parallel as the friction line so it is the planar side of the hull.

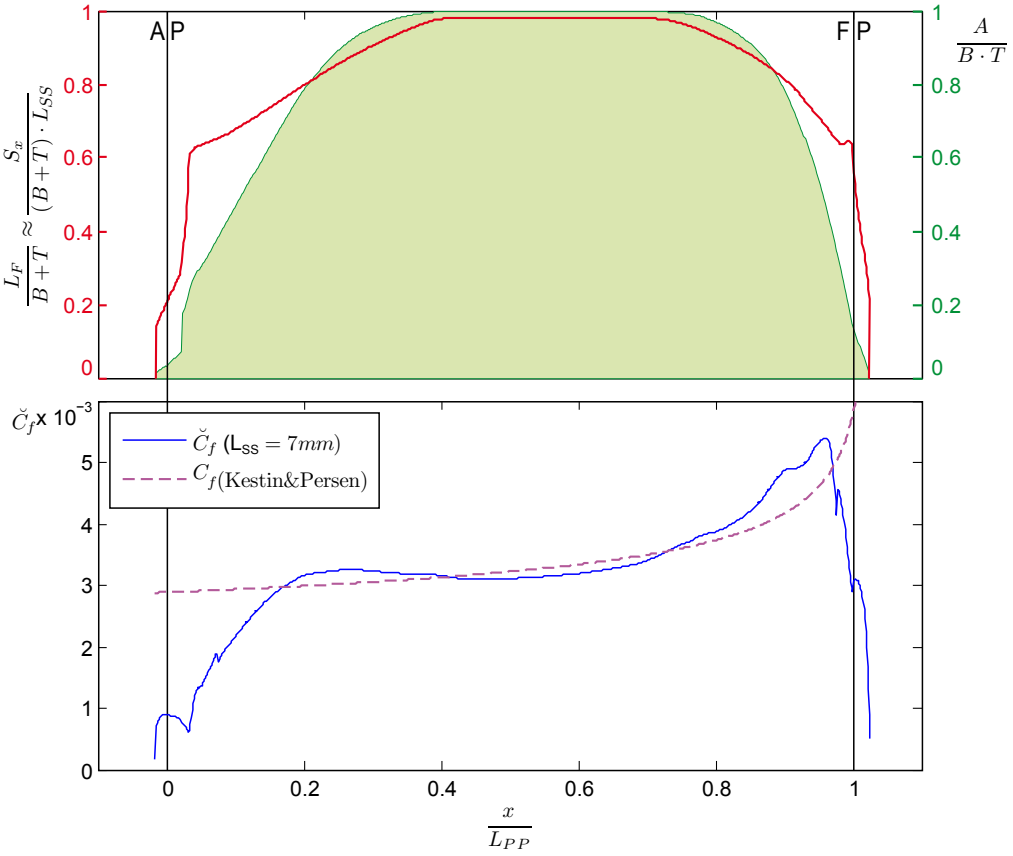

Figure 5.7: Station friction coefficient distribution the length of the **KVLCC2 in model** scale.

The averaged friction along the frame $\breve{C}_f$ is plotted on figure 5.7. The behavior of this curve is closer to a flat plate. The linear correlation between the curves is 0.903 if only the parallel middle body is considered. The run body decreases the friction towards the stern.

5.4 Shear stress distribution in full scale

The distribution of the friction coefficient in full scale is similar to the model scale hull. There is larger influence of the flow coming in the keel from the bottom 5.8. The stress on the entry body has similar distribution but the shoulder have increased shear effects.

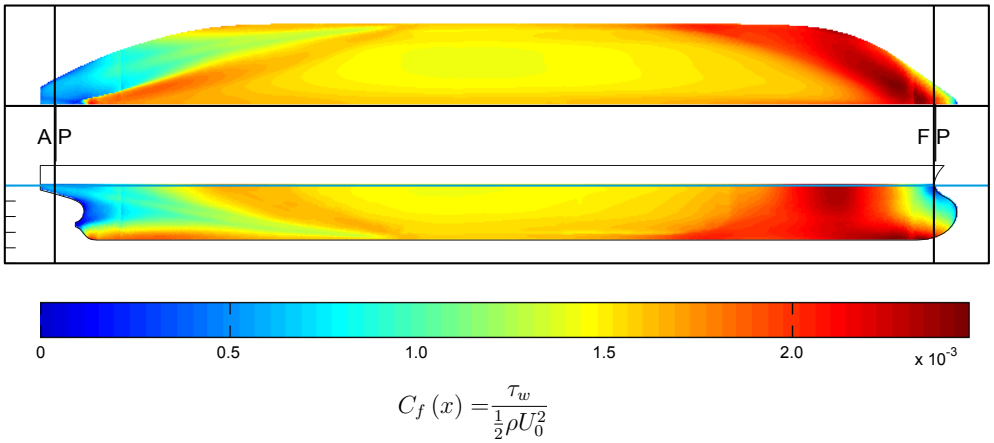

Figure 5.8: Friction coefficient distribution on the surface of the **KVLCC2 in full** scale.

The cuts of the hull plotted on figure 5.9 show the same results as the surface plot. The friction coefficient is closer to the friction line by Kestin and Persen 2.18. The water line cuts (constant z) reflect again the influence of the parallelt middle body on the friction distribution.

The figure 5.10 plots the frame averaged friction coefficient compared to the friction line. The full scale hull has higher $\breve{C}_f$ than the friction line, with less pronounced values on the shoulders when compared to the model scale. It is also posible to appreciate the decrease of shear stresses towards the stern.

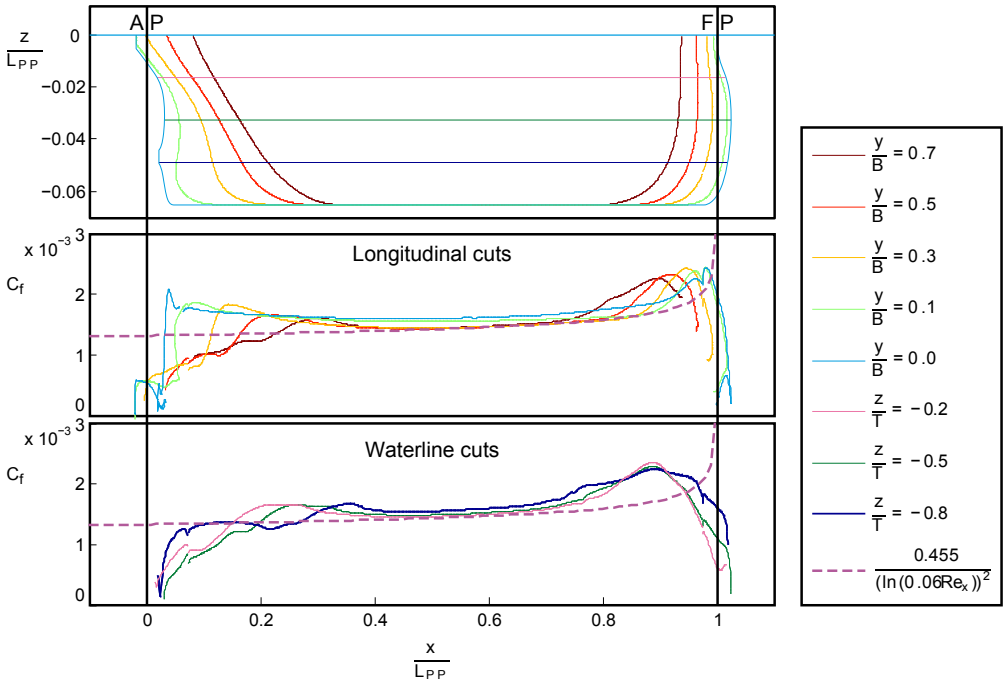

Figure 5.9: Friction coefficient distribution along water lines and longitudinal cuts of the **KVLCC2 in full** scale.

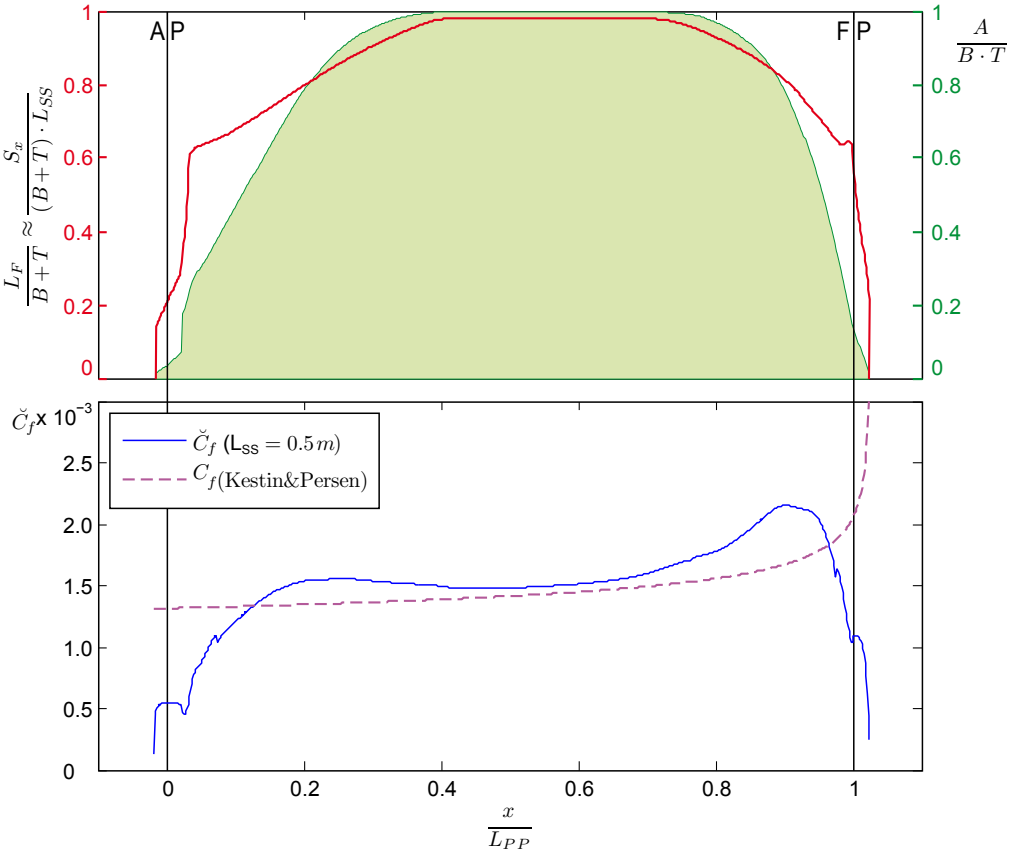

Figure 5.10: Station friction coefficient distribution the length of the **KVLCC2 in full** scale.

Chapter 6

Results on the cruise ferry hull

The cruise ferry hull described in chapter 3 has different division than the KVLCC2. The hull shape has only entry and run bodies both having approximately the same length. The lack of free surface computation leads to small uncertainty on the upper part of the bulbous bow. This is a pierced wave bulbous design but the upper boundary is a plane. Therefore the pierced wave is not represented in the domain.

The turbulence values 6.1 are based on the formula 5.6, which was validated with the results of the KVLCC2 in 5.

Size	Full scale	Model scale
Scale	1.0	$1:22.713$
$L = L_{PP}(m)$	200.8	8.8496
Test conditions		
$U_0\left(\frac{m}{s}\right)$	10.8033	2.2668
Re	$2.21 \cdot 10^9$	$20.06 \cdot 10^6$
I	3.5%	
$k\,(m^2 s^{-2})$	0.2144	$9.4421 \cdot 10^{-3}$
$\omega\,(s^{-1})$	0.5380	2.5615

Table 6.1: Flow conditions of the cruise ferry case.

6.1 Shear stress distribution in model scale

The entry and run bodies are much longer than the tanker case. This way, the flow is adapting along the shoulders (see figure 6.1). The distribution of shear stresses is smoother than the KVLCC2 case. There is a peak of the friction on the side of the bulbous bow. The friction on

the ceiling of the stern decreases in a more gradual pattern than the tanker.

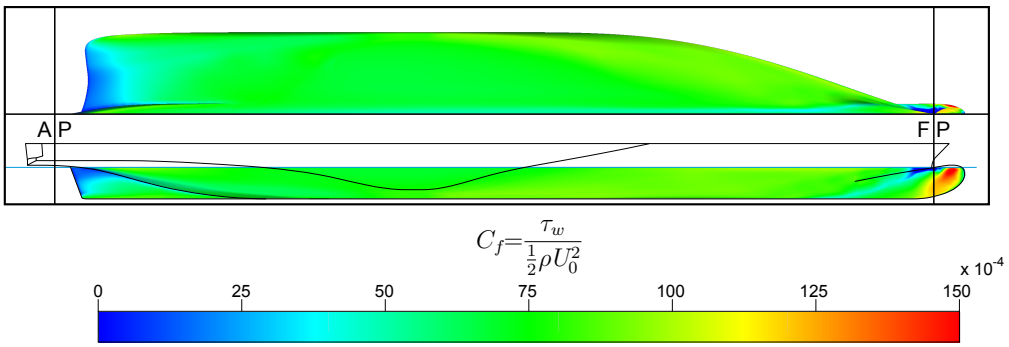

Figure 6.1: Friction coefficient distribution on the surface of the **cruise ship in model** scale.

The figure 5.6 contains the evolution of the friction coefficient along longitudinal cuts. Those are compared to the friction line of equation 2.18.

The longitudinal cuts different than the central plane (constant $y \neq 0$), fit well with the friction line by Kestin and Persen. The behavior of the shear stress is similar as the KVLCC2 on the shoulders. In this case, it is clear that the shear stress is higher until the effects of the shoulders are not important. The central cut is around 20% under the reference line with big increases in both the bulbous bow and the skeg. The water line cuts show the same behavior as the longitudinal cuts. The lack of free surface result in some random results on the upper cuts of the bulbous bow.

The figure 6.3 presents the averaged friction along the frame $\breve{C}_f$. The evolution of $\breve{C}_f$ for the cruise ferry is more gradual than the KVLCC2. There is a big peak on the bulbous followed by a stepped drop before the curve shows a smooth evolution. The curve on the amidship is over the reference friction line. The lack of parallel middle body explains this effect since the tanker is below the reference curve along the parallel body.

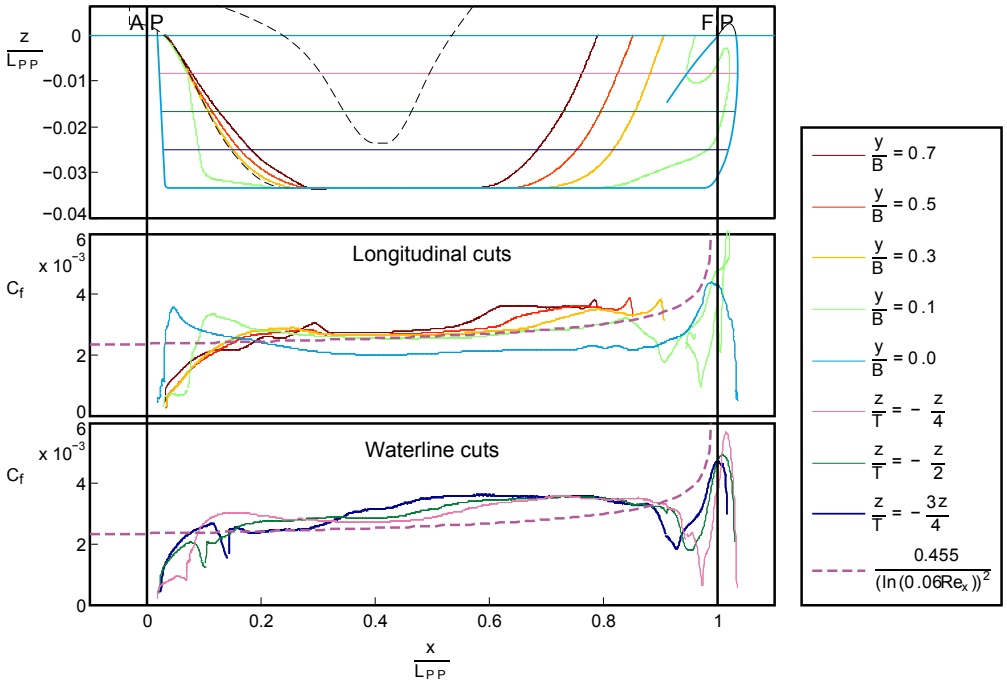

Figure 6.2: Friction coefficient distribution along water lines and longitudinal cuts of the **cruise ship in model** scale.

6.2 Shear stress distribution in full scale

The distribution of the friction coefficient in full scale 6.4 is more pronounced on the entry body than the model scale case. So is the effects of the upcoming flow on the skeg. On the other hand, the friction on the ceiling of the stern is not as marked as on the model.

Once again, the cuts on the hull evidence the same results as the model scale, as seen on figure 5.9. As in the tanker case, the friction coefficient is closer to the friction line.

The figure 5.10 with the frame averaged friction coefficient manifests the same results as the model scale.

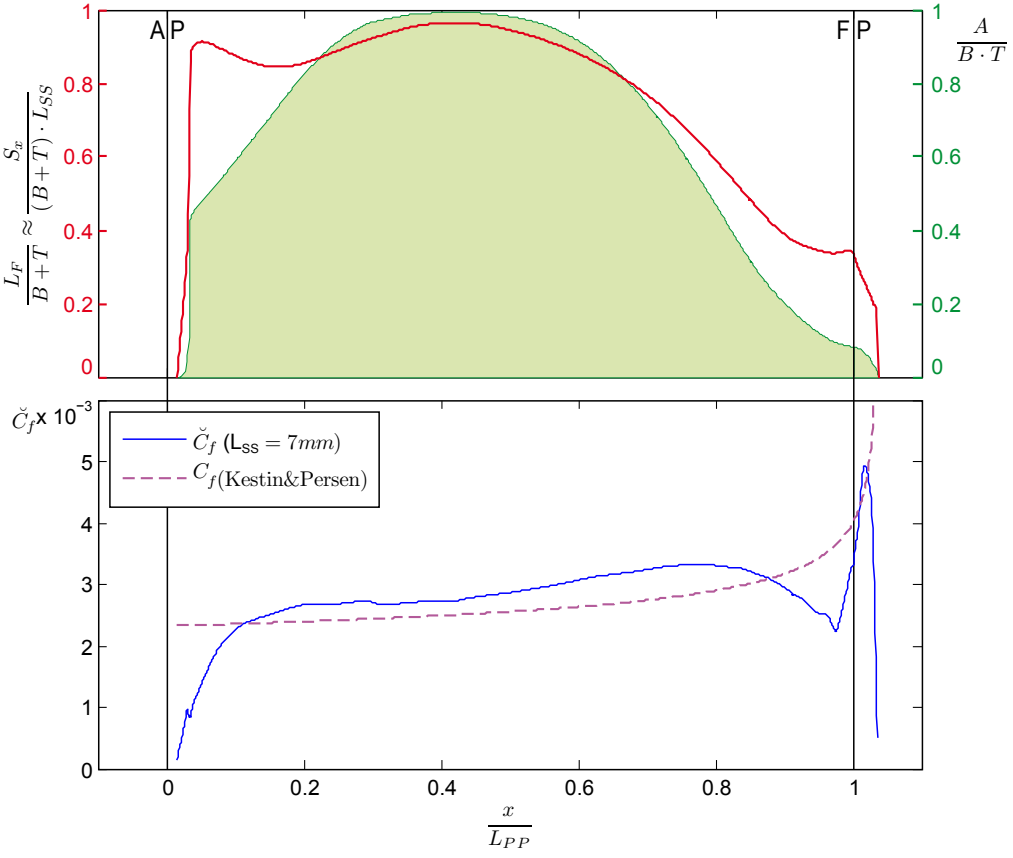

Figure 6.3: Station friction coefficient distribution the length of the **cruise ship in model** scale.

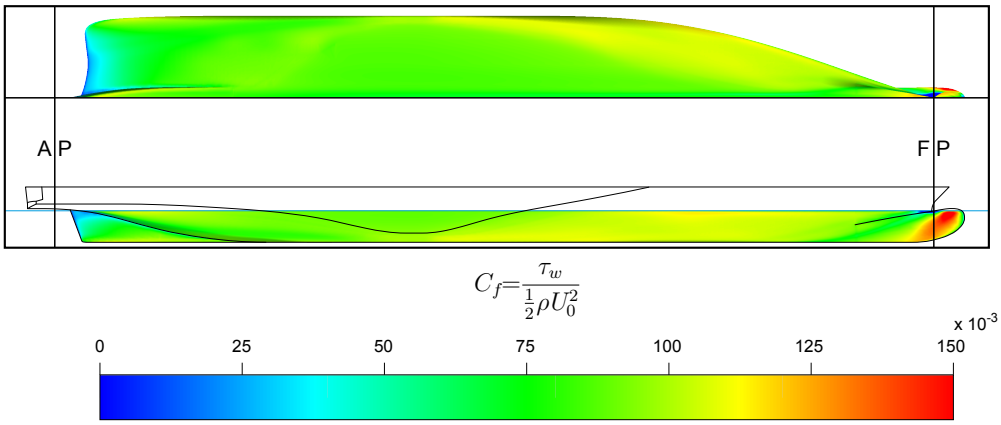

Figure 6.4: Friction coefficient distribution on the surface of the **cruise ship in full** scale.

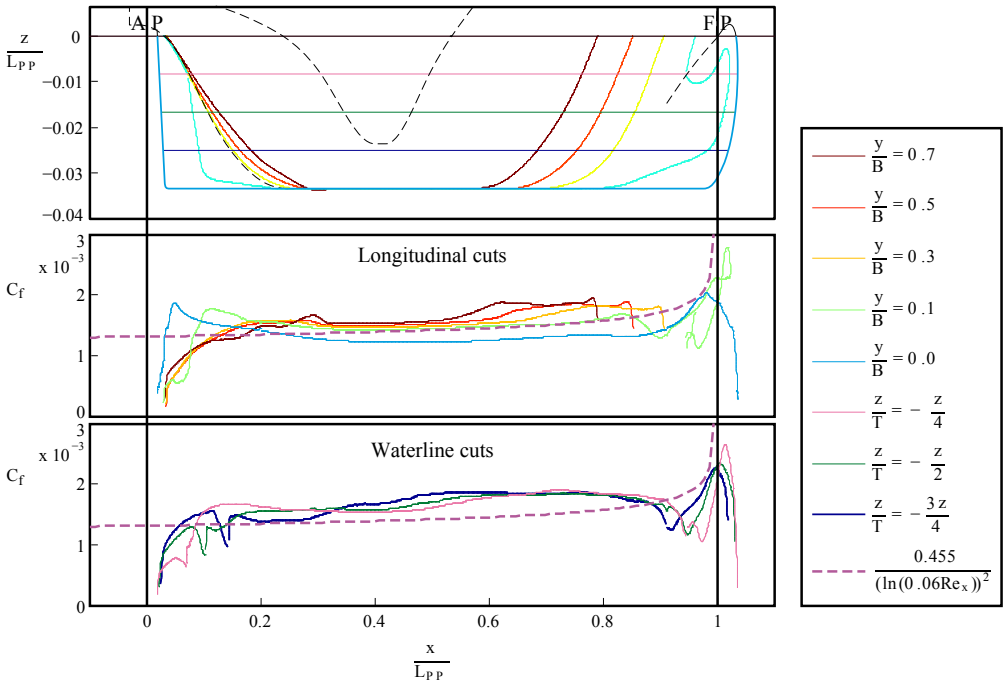

Figure 6.5: Friction coefficient distribution along water lines and longitudinal cuts of the **cruise ship in full** scale.

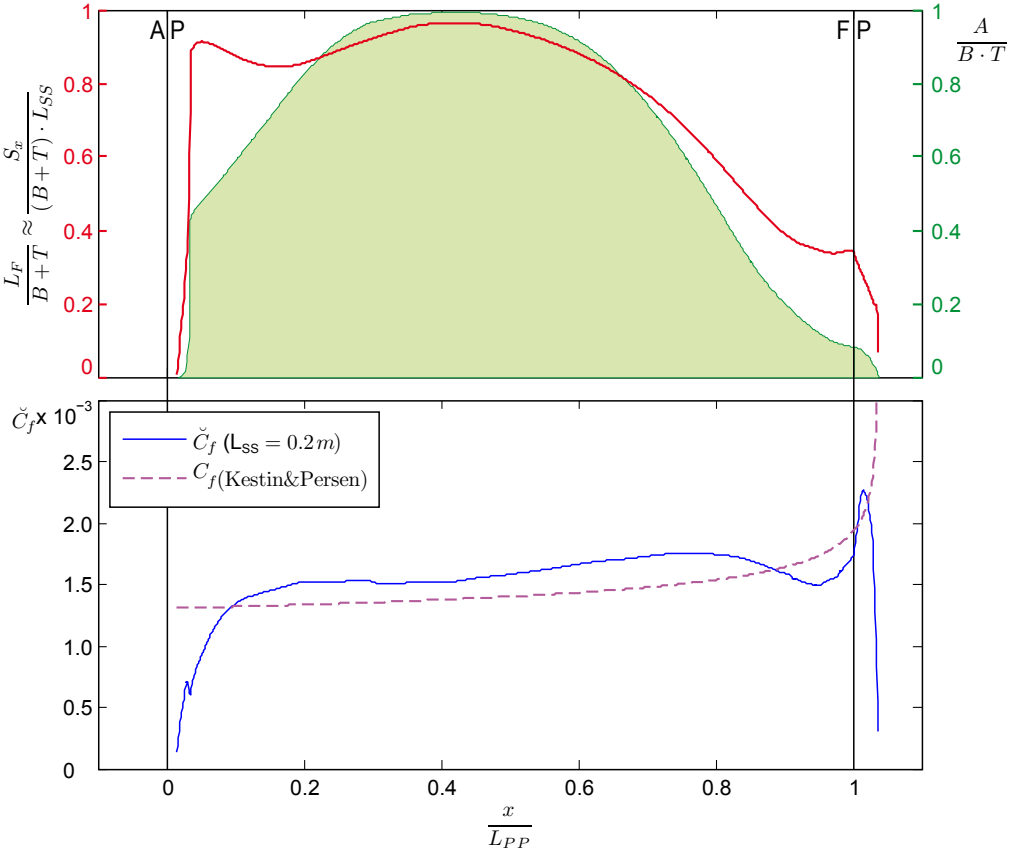

Figure 6.6: Station friction coefficient distribution the length of the **cruise ship in full** scale.

Chapter 7

Discussion

The results of the total resistance listed in table 7.1 show the hull form factors $(1+k)$ of both hulls in model and full scale. This value calculated with formula 2.27 is used to correlate the friction resistance between the model scale and the hull scale. Therefore, the value of the same hull should be similar in both model and full scale. This is not the case of the results obtained, where the values for the same hull have a large difference.

Case and scale	C_F	C_{PV}	C_T	C_{F0}	$1+k$
KVLCC2 model	3.387	0.9419	4.329	3.450	1.255
KVLCC2 full	1.576	0.6117	2.187	1.404	1.558
Cruise model	2.647	0.4112	3.058	2.668	1.146
Cruise full	1.471	0.2750	1.746	1.393	1.253

Table 7.1: Resistance components in coefficient form $(C \cdot 10^3)$ and hull form factor.

In order to make a deeper analysis, the friction resistance coefficient C_F is compared to the correlation line 2.26. The results in table 7.2 show that the values for model scale stay close to the correlation line (within 2%). On the other hand, the full scale results differ significantly from the ITTC57 line (over 12% difference for the KVLCC2).

7.1 Analysis of the correlation line with $\breve{C}_f$

The friction resistance coefficient is the average of the frame skin friction coefficient. The plots in figure 7.1 compare the distribution of the frame friction coefficient ($\breve{C}_f$) along the hull with the value of C_{F0}. As

Case	C_F	C_{F0}	$\frac{C_F}{C_{F0}}$
KVLCC2 model	$3.387 \cdot 10^{-3}$	$3.450 \cdot 10^{-3}$	98.2%
KVLCC2 full	$1.576 \cdot 10^{-3}$	$1.404 \cdot 10^{-3}$	112.2%
Cruise model	$2.647 \cdot 10^{-3}$	$2.668 \cdot 10^{-3}$	99.2%
Cruise full	$1.471 \cdot 10^{-3}$	$1.393 \cdot 10^{-3}$	105.5%

Table 7.2: Friction resistance coefficient compared to the correlation line.

seen in table 7.2, the average value of the friction coefficient in model scale (C_F) is very close to the correlation line (C_{F0}). The contribution on the entry body, which is over the correlated value, compensates the values below C_{F0} of the middle and run bodies.

From the upper plot in figure 7.1, it is posible to see two hulls with completely different distributions of shear stresses. But the correlated friction is based on the Reynolds number, which in these two cases has similar value ($Re_{Full} \approx 2 \cdot 10^9$). Therefore, the value of the correlated friction obviates the effects of the hull shape on the friction calculation.

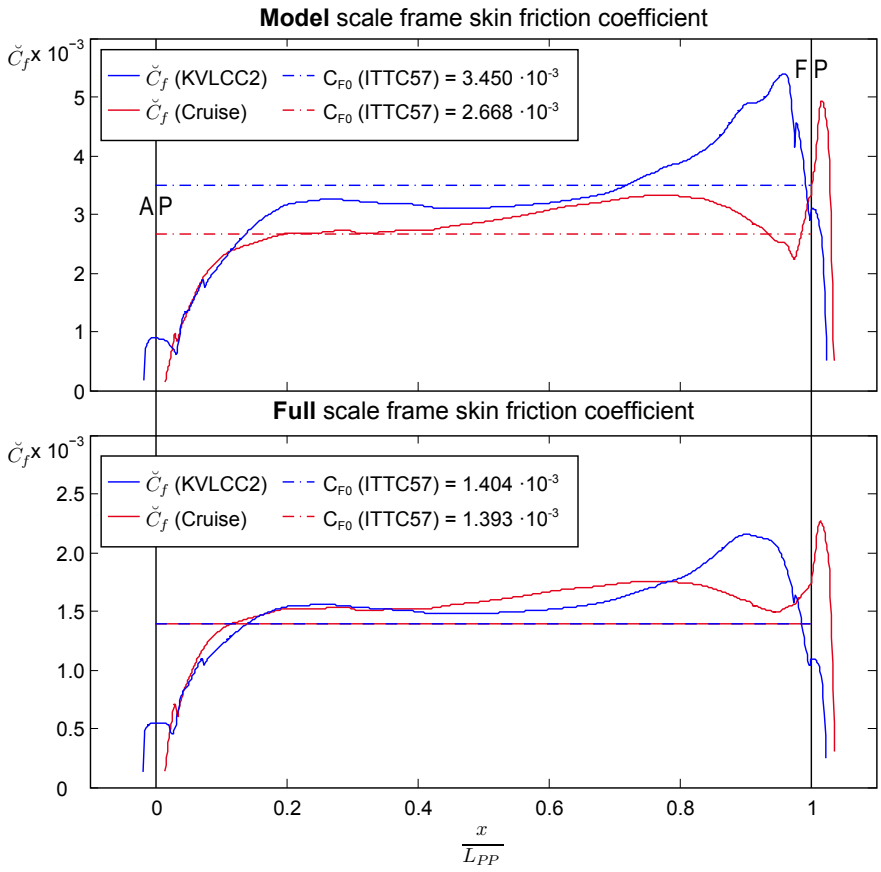

Figure 7.1: Comparison of the station friction coefficient distribution $\breve{C}_f$ on both hulls. The upper plot is for **model scale** and the lower for **full scale**.

7.2 Analysis of the form factor k with $\breve{C}_{PV}$

The hull form factor, $1+k$, represents the ratio between the viscous resistance and the friction resistance. The value 1 is, as seen in formula 2.27, the representation of the friction component and the the hull form factor k is, by definition, the ratio between the viscous pressure resistance coefficient, C_{POV} and the friction resistance C_{F0}. In order to see how the viscous pressure is distributed along the hulls, the frame averaged values $\breve{C}_{PV}$ are plotted in the figure 7.2.

The results show little information as the frame averaged viscous pressure coefficient, $\breve{C}_{PV}$, is one order of magnitude higher than the

total average, C_{PV}. This is explained with the relation of figures 2.4 and 2.3. In order to compare the viscous effects on the pressure distribution, it is necessary to subtract the non viscous effects, i.e. the potential flow around the hull. But this task would require a whole master thesis.

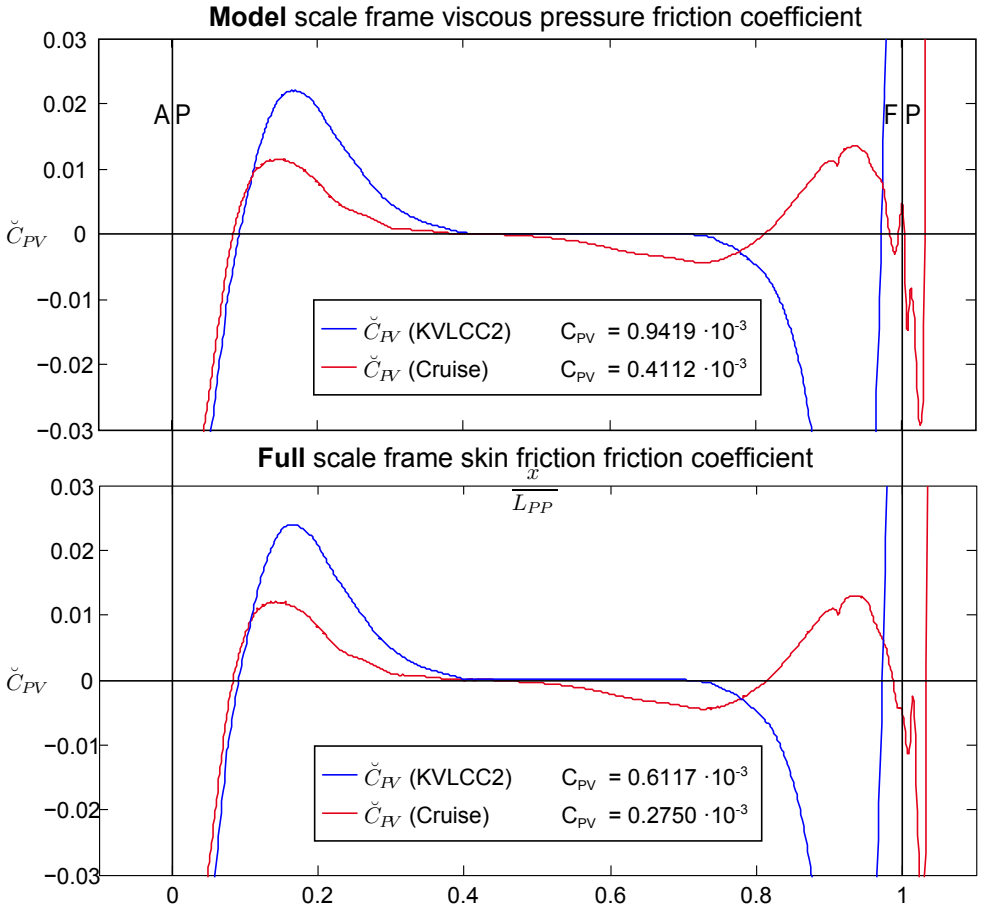

Figure 7.2: Comparison of the station viscous pressure coefficient distribution $\breve{C}_{PV}$ on both hulls. The upper plot is for **model scale** and the lower for **full scale**.

7.3 Future development of the present work

The study of shear stresses around two hulls has been focusing on the comparison with the ITTC procedures. The friction distribution has been linked to the length of the entry and run bodies. The influence of the hull shape is to be studied in order to optimize the future hulls.

The reliability of the actual CFD tools is good to split all the components of the resistance into smaller contributions. As suggested in section 7.2, the viscous pressure might be compared to the hull form factor, with the use of both turbulent viscous and potential flow theory.

The viscous effects with the free surface can be computed with a two fluid domain solver. The problems faced on the bulbous bow could be avoided if the free surface was implemented.

Chapter 8

Conclusions

In this section, the conclusions of the thesis are collected. These are split into conclusions of the results obtained and those of the performed tasks.

8.1 Conclusions of the results

The following conclusions from the work done can be divided in two: conclusions of the shear stress distributions and conclusions about the hull form factor.

Distribution of shear stresses

- The comparison of the shear stress development with a flat plate case is valid on the middle part of the hull. The length of the parallel middle body has low influence.
- The shoulders will increase the shear stresses when compared to a flat plate. When comparing both hulls there is a conclusion: the longer the entry body is, the smoother the effects of the shoulder are. The shear stresses on the run body do not depend on its extension, but rather on the shape. The transition on the aft shoulder is important. The shoulder of the tanker has small curvature (fast change) with the shear stresses peaking up and then down. On the other hand, the shoulder of the cruise ferry has larger curvature, decreasing the peak up. The parallel stern of the cruise ferry with skeg makes the shear stresses drop faster.
- The use of the ITTC57 correlation line is suitable as confirmed in model scale.

Hull form factor

- The hull form factor k can be confirmed to represent the viscous pressure resistance contribution. The results of chapter 7.2 show the influence of the resolution of the values.
- The hull form factor k is dependant on the scale. The ITTC procedures consider constant the hull form factor and correct the full scale resistance with other coefficients (C_A). The use of CFD as part of the resistance prediction could be use to determine the hull form factor at full scale.
- The viscous effects on the wave resistance cannot be confirmed in this thesis, but it shall be a continuation of the present work.
- The relation between k with the hull shape is still not determined. A further study could be performed with a comparison between a viscous CFD solver and a potential flow CFD solver.

8.2 Conclusions of the tasks

The different tasks required to write this thesis were: set up of the problem, compute the results, post-process the data and analyse it. The time spent on the tasks is arranged in the same order. The settings of the problem required almost half of the time spent on the thesis. This task was alternated with the computations, to check all the settings were properly chosen. The post processing and the analysis are link together. Some of the analysis of the initial results required a deeper post process.

- The setting up is a common task in all the CFD computations. As this task is similar in every single computation, the process cannot be long. The biggest problem faced in this thesis was the meshing of the domain. The meshes created with OpenFOAM's snappyHexMesh do not have enough quality to achieve reliable results on shear stresses. The meshing tool developed by Numeca, HEXPRESS, provides the required grids for this study. Some minor problems can be encountered on the original geometry files, but those are solved with a general CAD software. Structured grid generation would be useful in the study of the viscous effects as it should capture the development of the boundary layer with high resolution.

- The values of the different variables should have a initial reference quantity. The boundary conditions are not supposed to be in-house knowledge. Specially those with less presence in literature as it is with the turbulence variables k and ω. Nevertheless, it is important to check that all these variables are correctly applied. The results may be volatile with small changes on the values chosen.

- The post process, mainly done with Matlab but also shell script, require lots of scripts. These coding part inherits lots of scripts, lines and functions developed on previous courses. One of the best qualities of OpenFOAM is that the results can be exported in a large variety of file formats.

- The longitudinal and water line cuts are useful to see the local value of the shear stress. The introduced coefficient $\breve{C}_f$ shows in a better way the evolution along the hull. The use with the viscous pressure might be appropriate if compared to the potential pressure.

Bibliography

[1] 26TH ITTC QUALITY SYSTEMS GROUP. Ittc symbols and terminology list. In *Recommended Procedures and Guidelines*, Iternational Towing Tank Conference.

[2] ASSOCIATION, U. P. D. *Initial Graphics Exchange Specification: IGES 5.3*. IGES/PDES Organization, South Carolina, USA, September 1996.

[3] BATCHELOR, G. K. *An introduction to fluid dynamics*. Cambridge university press, 2000.

[4] COLES, D. E., AND HIRST, E. A. *Computation of Turbulent Boundary Layers*, vol. 2. 1968.

[5] COURANT, R., FRIEDRICHS, K., AND LEWY, H. On the partial difference equations of mathematical physics. *IBM journal of Research and Development 11*, 2 (1967), 215–234.

[6] DENLI, N., AND LANDWEBER, L. Thick axisymmetric turbulent boundary layer on a circular cylinder. *Journal of Hydronautics*, 13 (1979).

[7] EÇA, L., AND HOEKSTRA, M. The numerical friction line. *Journal of marine science and technology 13*, 4 (2008), 328–345.

[8] EÇA, L., AND HOEKSTRA, M. Near-wall profiles of mean flow and turbulence quantities predicted by eddy-viscosity turbulence models. *International Journal for Numerical Methods in Fluids*, 63 (2010), 953:988.

[9] ESQUIVEL, P., AND MARTINI, M. Exercise 1 turbulent boundary layer in a channel. DTU course 41128 Turbulence Theory, October 6 2011.

[10] GANT, S. E. *Development and Application of a New Wall Function for Complex Turbulent Flows*. PhD thesis, University of Manchester. Institute of Science and Technology, November.

[11] GENERATOR, H. U. G. *User Manual*, v2.12c ed. NUmerical MEChanics Applications, Chaussée de la Hulpe, 189, Terhulpsesteenweg B-1170 Brussels. Belgium, August 2012.

[12] GUO, B., STEEN, S., AND DENG, G. Seakeeping prediction of KVLCC2 in head waves with RANS. *Applied Ocean Research 35* (2012), 56–67.

[13] HUGHES, G. Friction and form resistance in turbulent flow, and a proposed formulation for use in model and ship correlation, 1954.

[14] ISMAIL, F., CARRICA, P. M., XING, T., AND STERN, F. Evaluation of linear and nonlinear convection schemes on multidimensional non-orthogonal grids with applications to KVLCC2 tanker. *International Journal for Numerical Methods in Fluids 64*, 8 (2010), 850–886.

[15] ITTC 7.5-03-02-02. Resistance and flow benchmark database for cfd validation for resistance and propulsion. In *Recommended Procedures and Guidelines*, Iternational Towing Tank Conference.

[16] ITTC 7.5-03-02-03. Practical guidelines for ship CFD applications. In *Recommended Procedures and Guidelines*, Iternational Towing Tank Conference.

[17] KATSUI, T., ASAI, H., HIMENO, Y., AND TAHARA, Y. The proposal of a new friction line. In *Fifth Osaka colloquium on advanced CFD applications to ship flow and hull form design, Osaka, Japan* (2005).

[18] KIM, K. C.; LEE, Y., AND MA, E., Eds. *An experimental study on the effect of transverse convex curvature on turbulent flow and heat transfer* (Beijing, 1990), Proceedings of the First International Symposium on Experimental and Computational Aerothermodynamics of Internal Flows.

[19] KRISO. Kvlcc2 description and wind tunnel data. Web page, 2005.

[20] LARSSON, L., STERN, F., AND BERTRAM, V. Benchmarking of computational fluid dynamics for ship flows: The gothenburg 2000 workshop. *Journal of Ship Research 47*, 1 (2003), 63–81.

[21] LARSSON, L., STERN, F., AND VISONNEAU, M. Gothenburg 2010, a workshop on numerical ship hydrodynamics. Tech. rep., Chalmers University of Technology. Institutionen för sjöfart och marin teknik, Hydromekanik, December 2010.

[22] MENTER, F., AND ESCH, T. Elements of industrial heat transfer predictions. In *16th Brazilian Congress of Mechanical Engineering* (November 2001), COBEM.

[23] MENTER, F. R. Zonal two equation kappa-omega turbulence models for aerodynamic flows. *c1993 1* (1993).

[24] OPENFOAM FUNDATION. Openfoam user guide. From webpage, May 2012.

[25] REE, J. H., AND MOORE, D. Experimental investigations of the compressible turbulent boundary layer at very high reynolds numbers. *AIAA Journal 3*, 4 (1965), 631–638.

[26] RESISTANCE COMITEE. Proceedings of the 8th ITTC. Iternational Towing Tank Conference.

[27] RESISTANCE COMITEE. Proceedings of the 148th ITTC. In *Form factor according to Prohaska* (Ottawa, Canada, 1975), Iternational Towing Tank Conference.

[28] RINA. The royal institution of naval architects 1860 - 2010. Web page, 2010.

[29] SCHLICHTING, H., KESTIN, J., SCHLICHTING, H., AND SCHLICHTING, H. *Boundary-layer theory*, vol. 539. McGraw-Hill New York, 1968.

[30] SCHOENHERR, K. E. Resistance of flat surfaces moving thorugh a fluid, 1932.

[31] SOFTWARE, S. I. Parasolid. 2001.

[32] VAN, S., ET AL. Technology for enhancing resistance performance of ships. *KRISO Report, November* (1998).

[33] WHITE, F. M. *Viscous fluid flow*, 3 ed. 2006.

[34] WINTER, K. G., AND GAUDET, L. *Turbulent boundary-layer studies at high Reynolds numbers at Mach numbers between 0.2 and 2.8*. HM Stationery Office, 1973.

List of Tables

List of Figures

Comments on the figures

Figures 2.1, 2.2, 2.3, 2.4, 2.5, 2.7, 4.1 and 4.2 can be extracted from this document in **vector format** and transformed if desired.

Appendix A

OpenFOAM case

A.1 Directory structure

The structure of a case is very strict. OpenFOAM considers every file of the case as a dictionary of variables. Therefore, all the files have to respect the sintaxis of C++. The location of the files represented on figure A.1 goes as follows:

The solver properties are located in the system folder (see A.2.1). Those properties are the time step, the save interval, the solvers (A.2.1.3), the numerical solvers selected (A.2.1.2), the discretization schemes(A.2.1.1), initial fields (A.2.1.4) and some other dictionaries.
There is the *constant* folder with all the constants like the fluid properties (see A.2.2) or the mesh grid (this is a static mesh problem). The mesh grid is to be located in the polyMesh folder. In case it was generated with snappyHexMesh, the STL mesh surface is located in *triSurface*.
The boundaries are defined in the polyMesh folder, but the boundary conditions are defined in each time directory (or at least in the first time step, see A.2.3). Each time step saved creates a new time directory.

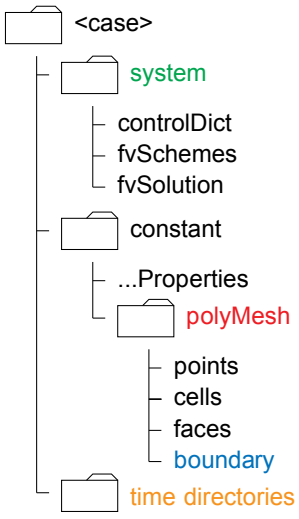

Figure A.1: OpenFOAM directory structure. Source: [24]

A.2 File examples

A.2.1 System variables of the solver

A.2.1.1 fvSchemes

```
/*---------------------------------*- C++ -*----------------------------------*\
| =========                 |                                                 |
| \\      /  F ield         | OpenFOAM: The Open Source CFD Toolbox           |
|  \\    /   O peration     | Version:  2.1.1                                 |
|   \\  /    A nd           | Web:      www.OpenFOAM.org                      |
|    \\/     M anipulation  |                                                 |
\*---------------------------------------------------------------------------*/
FoamFile
{   version     2.0;
    format      ascii;
    class       dictionary;
    location    "system";
    object      fvSchemes;
}
// * * * * * * * * * * * * * * * * * * * * * * * * * * * * * * * * * * * * * //
ddtSchemes
{   default         Euler;}
gradSchemes
{   default         Gauss linear;}
divSchemes
{
    default         none;
    div(phi,U)      Gauss linearUpwindV grad(U);
    div(phi,k)      Gauss limitedLinear 1;
    div(phi,omega)  Gauss limitedLinear 1;
    div(phi,R)      Gauss limitedLinear 1;
    div(R)          Gauss linear;
    div(phi,nuTilda) Gauss limitedLinear 1;
    div((nuEff*dev(T(grad(U))))) Gauss linear;
}
laplacianSchemes
{   default         Gauss linear corrected;}
interpolationSchemes
{   default         linear;}
snGradSchemes
{   default         corrected;}
fluxRequired
{   default         no;
    p;}
```

A.2.1.2 fvSolution

```
FoamFile
{    version     2.0;
     format      ascii;
     class       dictionary;
     location    "system";
     object      fvSolution;}
// * * * * * * * * * * * * * * * * * * * * * * * * * * * * * * * * * * * * * * * * * * * * * * * * * * * * * * * * //
solvers
{    p
     {solver           GAMG;
      tolerance        1e-7;
      relTol           0.1;
      smoother         GaussSeidel;
      nPreSweeps       0;
      nPostSweeps      2;
      cacheAgglomeration on;
      agglomerator     faceAreaPair;
      nCellsInCoarsestLevel 10;
      mergeLevels      1;}
     U
     {solver           smoothSolver;
      smoother         GaussSeidel;
      tolerance        1e-8;
      relTol           0.1;
      nSweeps          1;}
     k
     {solver           smoothSolver;
      smoother         GaussSeidel;
      tolerance        1e-8;
      relTol           0.1;
      nSweeps          1;}
     omega
     {solver           smoothSolver;
      smoother         GaussSeidel;
      tolerance        1e-8;
      relTol           0.1;
      nSweeps          1;}
}
SIMPLE
{    nNonOrthogonalCorrectors 0;}
potentialFlow
{    nNonOrthogonalCorrectors 10;}
relaxationFactors
{    fields
     {p               0.3;}
     equations
     {U               0.7;
      k               0.7;
      omega           0.7;}
}
cache
{     grad(U);}
```

A.2.1.3 controlDict

```
/*--------------------------------*- C++ -*----------------------------------*\
| =========                 |                                                 |
| \\      /  F ield         | OpenFOAM: The Open Source CFD Toolbox           |
|  \\    /   O peration     | Version:  2.1.1                                 |
|   \\  /    A nd           | Web:      www.OpenFOAM.org                      |
|    \\/     M anipulation  |                                                 |
\*---------------------------------------------------------------------------*/
FoamFile
{   version     2.0;
    format      ascii;
    class       dictionary;
    location    "system";
    object      controlDict;} // ************************************************
application     LTSInterFoam;
startFrom       startTime;
startTime       0;
stopAt          endTime;
endTime         30;    // The time in seconds, check convergence of forces file
deltaT          0.005; // 0.005 = 0.001*L/U
writeControl    timeStep;
writeInterval   2.0;   // Save every 2 sec of computed time
purgeWrite      0;
writeFormat     ascii;
writePrecision  6;
writeCompression compressed;
timeFormat      general;
timePrecision   6;
runTimeModifiable yes;
functions // ************* More functions in motorbike tutorial ***************
(       forces
    {           type forces;
                functionObjectLibs ("libforces.so"); //Lib to load
                outputControl   timeStep;
                outputInterval 1;
                patches (hull_surface); // patch to measure forces from
                rhoInf 1000; //Reference density for fluid
                nuInf 1e-6; //Reference kinetic viscosity for fluid
                CofR (0 0 0); //Origin for moment calculations }
        forceCoeffs
        {type forceCoeffs;
         functionObjectLibs ("libforces.so");
         outputControl   timeStep;
         outputInterval 1;
         patches ("hull_surface.*"); // for many patches use ("hull_surface.*")
         rhoName rhoInf;
         rhoInf 1000;
         nuInf 1e-6;
         CofR (0 0 0);
         liftDir (0 0 1);
         dragDir (-1 0 0); // The negative is to have a positive resistance.
         pitchAxis (0 1 0);
         magUInf   1.047; // Re4.6e6 (nu = 1.256e-6)
         lRef      5.5172;
         Aref      4.117;}
);
```

A.2.1.4 setFieldsDict

This file is only necessary with `interFoam`. It sets the initial field of water and air.

```
/*--------------------------------*- C++ -*----------------------------------*\
| =========                 |                                                 |
| \\      /  F ield         | OpenFOAM: The Open Source CFD Toolbox           |
|  \\    /   O peration     | Version:  2.1.1                                 |
|   \\  /    A nd           | Web:      www.OpenFOAM.org                      |
|    \\/     M anipulation  |                                                 |
\*---------------------------------------------------------------------------*/
FoamFile
{   version     2.0;
    format      ascii;
    class       dictionary;
    location    "system";
    object      setFieldsDict; } // ************************************
defaultFieldValues
(   volScalarFieldValue alpha1 0 );
regions
(   boxToCell
    {   box (-100 -100 -100) (100 100 -5); //0
        fieldValues
        (   volScalarFieldValue alpha1 1 );
    }
);
```

A.2.1.5 decomposeParDict

This file is used to decompose the problem for parallel computing.

```
/*--------------------------------*- C++ -*----------------------------------*\
| =========                 |                                                 |
| \\      /  F ield         | OpenFOAM: The Open Source CFD Toolbox           |
|  \\    /   O peration     | Version:  2.1.1                                 |
|   \\  /    A nd           | Web:      www.OpenFOAM.org                      |
|    \\/     M anipulation  |                                                 |
\*---------------------------------------------------------------------------*/
FoamFile
{
    version     2.0;
    format      ascii;
    class       dictionary;
    location    "system";
    object      decomposeParDict; } // ************************************
numberOfSubdomains 12; // 12=3*2*2
method             hierarchical;
hierarchicalCoeffs  // 3 in X 2 in Y and 2 inZ
{   n               ( 3 2 2 );
    delta           0.001;
    order           xyz; // It could be yxz meaning 3 in Y first
}
distributed     no;
roots           ( ); // No idea
```

A.2.1.6 mapFieldsDict

Example for mapping two different meshes.

```
/*--------------------------------*- C++ -*----------------------------------*\
| =========                 |                                                 |
| \\      /  F ield         | OpenFOAM: The Open Source CFD Toolbox           |
|  \\    /   O peration     | Version:  2.1.1                                 |
|   \\  /    A nd           | Web:      www.OpenFOAM.org                      |
|    \\/     M anipulation  |                                                 |
\*---------------------------------------------------------------------------*/
FoamFile
{
    version     2.0;
    format      ascii;
    class       dictionary;
    location    "system";
    object      mapFieldsDict;
}
// * * * * * * * * * * * * * * * * * * * * * * * * * * * * * * * * * * * * //
patchMap        (ceiling_a bottom_a inlet_w portside_w outlet crujia);
cuttingPatches  ("hull_surface.*");

/*---------------------------------------------------------------------------*\
|  The working directory is below both cases i.e.:                            ↩
    |
|  cd $WRKDIR/OpenFOAM/esquivel-2.1.x/run                                     ↩
    |
|  inside run there are two folders with the cases ship_origin and ship_to_map ↩
    |
|  The file mapFieldsDict is located in the folder ship_to_map/system/        ↩
    |
|  The command to run it is:                                                  ↩
    |
|  mapFields ship_origin -case ship_to_map -sourceTime latestTime             ↩
    |
\*---------------------------------------------------------------------------*/
```

A.2.2 Constant variables

```
/*--------------------------------*- C++ -*----------------------------------*\
| =========                 |                                                 |
| \\      /  F ield         | OpenFOAM: The Open Source CFD Toolbox           |
|  \\    /   O peration     | Version:  2.1.1                                 |
|   \\  /    A nd           | Web:      www.OpenFOAM.org                      |
|    \\/     M anipulation  |                                                 |
\*---------------------------------------------------------------------------*/
FoamFile
{   version     2.0;
    format      ascii;
    class       uniformDimensionedVectorField;
    location    "constant";
    object      g; }   //*************************************************
dimensions      [0 1 -2 0 0 0 0];
value           (0 0 -9.81);
```

```
/*--------------------------------*- C++ -*----------------------------------*\
| =========                 |                                                 |
| \\      /  F ield         | OpenFOAM: The Open Source CFD Toolbox           |
|  \\    /   O peration     | Version:  2.1.1                                 |
|   \\  /    A nd           | Web:      www.OpenFOAM.org                      |
|    \\/     M anipulation  |                                                 |
\*---------------------------------------------------------------------------*/
FoamFile
{    version     2.0;
     format      ascii;
     class       dictionary;
     location    "constant";
     object      RASProperties; } //*****************************************
RASModel        kOmegaSST;
turbulence      on;
printCoeffs     on;
```

```
/*--------------------------------*- C++ -*----------------------------------*\
| =========                 |                                                 |
| \\      /  F ield         | OpenFOAM: The Open Source CFD Toolbox           |
|  \\    /   O peration     | Version:  2.1.1                                 |
|   \\  /    A nd           | Web:      www.OpenFOAM.org                      |
|    \\/     M anipulation  |                                                 |
\*---------------------------------------------------------------------------*/
FoamFile
{    version     2.0;
     format      ascii;
     class       dictionary;
     location    "constant";
     object      turbulenceProperties; } //*********************************
simulationType  turbulent;
```

```
/*--------------------------------*- C++ -*----------------------------------*\
| =========                 |                                                 |
| \\      /  F ield         | OpenFOAM: The Open Source CFD Toolbox           |
|  \\    /   O peration     | Version:  2.1.1                                 |
|   \\  /    A nd           | Web:      www.OpenFOAM.org                      |
|    \\/     M anipulation  |                                                 |
\*---------------------------------------------------------------------------*/
FoamFile
{    version     2.0;
     format      ascii;
     class       dictionary;
     location    "constant";
     object      transportProperties; }
// * * * * * * * * * * * * * * * * * * * * * * * * * * * * * * * * * * * * //
transportModel  Newtonian;
nu              nu [0 2 -1 0 0 0 0] 1.256e-06;
```

A.2.3 Initial time variables

```
/*---------------------------------*- C++ -*----------------------------------*\
| =========                 |                                                 |
| \\      /  F ield         | OpenFOAM: The Open Source CFD Toolbox           |
|  \\    /   O peration     | Version:  2.1.1                                 |
|   \\  /    A nd           | Web:      www.OpenFOAM.org                      |
|    \\/     M anipulation  |                                                 |
\*---------------------------------------------------------------------------*/
FoamFile
{   version     2.0;
    format      ascii;
    class       volVectorField;
    location    "0";
    object      U;}
// * * * * * * * * * * * * * * * * * * * * * * * * * * * * * * * * * * * * * * * //

dimensions      [0 1 -1 0 0 0 0]; // m/s

internalField   uniform (-1.047 0 0); // KVLCC2 scale 1:58 Re=4.6e6

boundaryField //
{
    inlet_w // Water                    inflowWater
    {   type            fixedValue;
        value           uniform (-1.047 0 0);
    }
    outlet // outlet                    outflow
    {   type            zeroGradient;}

    ceiling_a // abaft                  ceiling
    {   type            slip;}

    crujia // CenterLine                center
    {  type           symmetryPlane; }

    bottom_a // abaft                   bottom
    {  type           zeroGradient; }

    portside_w
    {   type            slip;}

    hull_surface.abaft
    {   type            fixedValue;
        value           uniform (0 0 0);
    }
    hull_surface.body
    {   type            fixedValue;
        value           uniform (0 0 0);
    }
    hull_surface.bow
    {   type            fixedValue;
        value           uniform (0 0 0);
    }
}
// ************************************************************************* //
```

```
/*--------------------------------*- C++ -*----------------------------------*\
| =========                 |                                                 |
| \\      /  F ield         | OpenFOAM: The Open Source CFD Toolbox           |
|  \\    /   O peration     | Version:  2.1.1                                 |
|   \\  /    A nd           | Web:      www.OpenFOAM.org                      |
|    \\/     M anipulation  |                                                 |
\*---------------------------------------------------------------------------*/
FoamFile
{
    version     2.0;
    format      ascii;
    class       volScalarField;
    object      p;
}
// * * * * * * * * * * * * * * * * * * * * * * * * * * * * * * * * * * * * * * * * * * * * //

pressure        0;  // This value changes all the presure

dimensions      [0 2 -2 0 0 0 0]; // Specific pressure (m^2/s^2)

internalField   uniform $pressure;

boundaryField //                        Tuomas Polvi
{
    inlet_w // Water                        inflowWater
    {   type            zeroGradient;}

    outlet // outlet                        outflow
    {   type        fixedValue;
    value       uniform $pressure;}

    ceiling_a // abaft                      ceiling
    {   type            zeroGradient;}

    crujia // CenterLine                    center
    {  type            symmetryPlane; }

    bottom_a // abaft                       bottom
    {   type            zeroGradient;} // =slip

    portside_w
    {   type            zeroGradient;} // =slip

    hull_surface.abaft
    {   type            zeroGradient;} // =slip
    hull_surface.body
    {   type            zeroGradient;} // =slip
    hull_surface.bow
    {   type            zeroGradient;} // =slip
}

// ************************************************************************* //
```

```
/*--------------------------------*- C++ -*----------------------------------*\
| =========                 |                                                 |
| \\      /  F ield         | OpenFOAM: The Open Source CFD Toolbox           |
|  \\    /   O peration     | Version:  2.1.0                                 |
|   \\  /    A nd           | Web:      www.OpenFOAM.org                      |
|    \\/     M anipulation  |                                                 |
\*---------------------------------------------------------------------------*/
FoamFile
{
    version     2.0;
    format      ascii;
    class       volScalarField;
    location    "0";
    object      nut;
}
// * * * * * * * * * * * * * * * * * * * * * * * * * * * * * * * * * * * * * * * //
nut_value  1.0E-08;

dimensions      [0 2 -1 0 0 0 0];
internalField   uniform  $nut_value;

boundaryField
{
    inlet_w // Water = 1
    {   type            fixedValue;
        value           uniform $nut_value;
    }

    outlet // OUTLET, price discount!!!
    {  type            zeroGradient; }

    ceiling_a // abaft
    {  type            zeroGradient; }

    bottom_a // abaft
    {  type            zeroGradient; }

    portside_w
    {  type            zeroGradient; }

    crujia // CenterLine
    {  type     symmetryPlane; }

    "hull_surface.*"
    {   type            nutkWallFunction;
        value           uniform 0;
    }
}
// ************************************************************************* //
```

```
/*--------------------------------*- C++ -*----------------------------------*\
| =========                 |                                                 |
| \\      /  F ield         | OpenFOAM: The Open Source CFD Toolbox           |
|  \\    /   O peration     | Version:  2.1.0                                 |
|   \\  /    A nd           | Web:      www.OpenFOAM.org                      |
|    \\/     M anipulation  |                                                 |
\*---------------------------------------------------------------------------*/
FoamFile
{
    version     2.0;
    format      ascii;
    class       volScalarField;
    location    "0";
    object      k;
}
// * * * * * * * * * * * * * * * * * * * * * * * * * * * * * * * * * * * * * //
turbulentKE  0.002014284; // k=3/2*(U*I)^2  I=3.5%

dimensions      [0 2 -2 0 0 0 0];

internalField   uniform $turbulentKE;

boundaryField
{
    inlet_w // Water = 1
    {   type            fixedValue;
        value           uniform $turbulentKE;
    }
    outlet // outlet
    {  type            zeroGradient; }

    ceiling_a // abaft
    {  type            zeroGradient; }

    bottom_a // abaft
    {  type            zeroGradient; }

    portside_w
    {  type            zeroGradient; }

    crujia // CenterLine
    {  type     symmetryPlane; }

    hull_surface.abaft
    {   type            kqRWallFunction;
        value           uniform 0;
    }
    hull_surface.body
    {   type            kqRWallFunction;
        value           uniform 0;
    }
    hull_surface.bow
    {   type            kqRWallFunction;
        value           uniform 0;
    }
}

// ************************************************************************* //
```

```
/*--------------------------------*- C++ -*----------------------------------*\
| =========                 |                                                 |
| \\      /  F ield         | OpenFOAM: The Open Source CFD Toolbox           |
|  \\    /   O peration     | Version:  2.1.0                                 |
|   \\  /    A nd           | Web:      www.OpenFOAM.org                      |
|    \\/     M anipulation  |                                                 |
\*---------------------------------------------------------------------------*/
FoamFile
{
    version     2.0;
    format      ascii;
    class       volScalarField;
    object      omega;
}
// * * * * * * * * * * * * * * * * * * * * * * * * * * * * * * * * * * * * * //
turbulentOmega  1.897701733; // = 10*U/Lpp

dimensions      [0 0 -1 0 0 0 0];

internalField   uniform $turbulentOmega;

boundaryField
{
    inlet_w // Water = 1
    {   type            fixedValue;
        value           uniform $turbulentOmega;
    }

    outlet // outlet
    {  type            zeroGradient; }

    ceiling_a // abaft
    {  type     zeroGradient; }

    bottom_a // abaft
    {  type     zeroGradient; }

    portside_w
    {  type     zeroGradient; }

    crujia // CenterLine
    {  type     symmetryPlane; }

    hull_surface.abaft
    {   type            omegaWallFunction;
        value           uniform $turbulentOmega;
//        value           uniform 1.25; // = 6*ny/(0.075*d^2)
    }
    hull_surface.body
    {   type            omegaWallFunction;
        value           uniform $turbulentOmega;
    }
    hull_surface.bow
    {   type            omegaWallFunction;
        value           uniform $turbulentOmega;
    }
}
// ************************************************************************* //
```

The next files are only for the free surface computations with `interFoam`.

```
/*--------------------------------*- C++ -*----------------------------------*\
| =========                 |                                                 |
| \\      /  F ield         | OpenFOAM: The Open Source CFD Toolbox           |
|  \\    /   O peration     | Version:  2.1.1                                 |
|   \\  /    A nd           | Web:      www.OpenFOAM.org                      |
|    \\/     M anipulation  |                                                 |
\*---------------------------------------------------------------------------*/
FoamFile
{   version     2.0;
    format      ascii;
    class       volScalarField;
    object      alpha;
}
// * * * * * * * * * * * * * * * * * * * * * * * * * * * * * * * * * * * * * //
dimensions      [0 0 0 0 0 0 0];

internalField   uniform 1;

boundaryField
{
    inlet_a // Air   = 0
    {   type            fixedValue;
        value           uniform 0;
    }
    inlet_w // Water = 1
    {   type        fixedValue;
        value       uniform 1;}
    outlet // OUTLET, price discount!!!
    {   type        zeroGradient; }
    ceiling_f // Ceiling fore
    {   type        fixedValue;
        value       uniform 0;}
    ceiling_a // abaft
    {   type        fixedValue;
        value       uniform 0;}
    bottom_f // Bottom fore
    {   type        fixedValue;
        value       uniform 1;}
    bottom_a // abaft
    {   type        fixedValue;
        value       uniform 1;}
    portside_a
    {   type        fixedValue;
        value       uniform 0;}
    portside_w
    {   type        fixedValue;
        value       uniform 1;}
    crujia // CenterLine
    {   type        symmetryPlane; }
    hull_surface
    {   type            zeroGradient; }
}
// ************************************************************************* //
```

```
/*--------------------------------*- C++ -*----------------------------------*\
| =========                 |                                                 |
| \\      /  F ield         | OpenFOAM: The Open Source CFD Toolbox           |
|  \\    /   O peration     | Version:  2.1.1                                 |
|   \\  /    A nd           | Web:      www.OpenFOAM.org                      |
|    \\/     M anipulation  |                                                 |
\*---------------------------------------------------------------------------*/
FoamFile
{
    version     2.0;
    format      ascii;
    class       volScalarField;
    object      p_rgh;
}
// * * * * * * * * * * * * * * * * * * * * * * * * * * * * * * * * * * * * * //

dimensions      [1 -1 -2 0 0 0 0];

internalField   uniform 0;

boundaryField //                        Tuomas Polvi
{
    inlet_w // Water                        inflowWater
    {   type            zeroGradient;}
    inlet_a // Air                      inflowAir
    {   type            zeroGradient;}

    outlet // OUTLET, price discount!!!            outflow
    {   type        fixedValue;
    value       uniform 0;}

    ceiling_f // Ceiling fore                  ceilingFront
    {   type        fixedValue;
    value       uniform 0;}
    ceiling_a // abaft                       ceiling
    {   type        fixedValue;
    value       uniform 0;}

    crujia // CenterLine                     center
    {  type           symmetryPlane; }

    bottom_a // abaft                        bottom
    {   type            zeroGradient;} // =slip
    bottom_f // Bottom fore                  bottomFrontAndSide
    {   type            zeroGradient;}

    portside_a //Portside, when it is in diagonal, works as inlet   side
    {   type            zeroGradient;} // =slip
    portside_w
    {   type            zeroGradient;} // =slip

    hull_surface //                     HULL_Wigley
    {   type            zeroGradient;} // =slip
}

// ************************************************************************* //
```